Adipocyte-Derived Lipids Mediate Melanoma Progression via FATP Proteins

Maomao Zhang[1], Julie S. Di Martino[2], Robert L. Bowman[1,3], Nathaniel R. Campbell[1,4,5], Sanjeethan C. Baksh[4], Theresa Simon-Vermot[1], Isabella S. Kim[1], Pearce Haldeman[1], Chandrani Mondal[2], Vladimir Yong-Gonzales[6], Mohsen Abu-Akeel[7], Taha Merghoub[7], Drew R. Jones[8], Xiphias Ge Zhu[9], Arshi Arora[10], Charlotte E. Ariyan[11], Kivanç Birsoy[9], Jedd D. Wolchok[7], Katherine S. Panageas[10], Travis Hollmann[12], Jose Javier Bravo-Cordero[2], and Richard M. White[1]

ABSTRACT

Advanced, metastatic melanomas frequently grow in subcutaneous tissues and portend a poor prognosis. Though subcutaneous tissues are largely composed of adipocytes, the mechanisms by which adipocytes influence melanoma are poorly understood. Using *in vitro* and *in vivo* models, we find that adipocytes increase proliferation and invasion of adjacent melanoma cells. Additionally, adipocytes directly transfer lipids to melanoma cells, which alters tumor cell metabolism. Adipocyte-derived lipids are transferred to melanoma cells through the FATP/SLC27A family of lipid transporters expressed on the tumor cell surface. Among the six FATP/SLC27A family members, melanomas significantly overexpress FATP1/SLC27A1. Melanocyte-specific FATP1 expression cooperates with $BRAF^{V600E}$ in transgenic zebrafish to accelerate melanoma development, an effect that is similarly seen in mouse xenograft studies. Pharmacologic blockade of FATPs with the small-molecule inhibitor Lipofermata abrogates lipid transport into melanoma cells and reduces melanoma growth and invasion. These data demonstrate that stromal adipocytes can drive melanoma progression through FATP lipid transporters and represent a new target aimed at interrupting adipocyte–melanoma cross-talk.

SIGNIFICANCE: We demonstrate that stromal adipocytes are donors of lipids that mediate melanoma progression. Adipocyte-derived lipids are taken up by FATP proteins that are aberrantly expressed in melanoma. Inhibition of FATPs decreases melanoma lipid uptake, invasion, and growth. We provide a mechanism for how stromal adipocytes drive tumor progression and demonstrate a novel microenvironmental therapeutic target. *Cancer Discov; 8(8); 1006–25. ©2018 AACR.*

Downloaded from http://aacrjournals.org/cancerdiscovery/article-pdf/8/8/1006/1841481/1006.pdf by guest on 27 August 2022

[1]Department of Cancer Biology and Genetics, Memorial Sloan Kettering Cancer Center, New York, New York. [2]Department of Medicine, Division of Hematology and Medical Oncology, Icahn School of Medicine, Tisch Cancer Institute at Mount Sinai, New York, New York. [3]Human Oncology and Pathogenesis Program, Memorial Sloan Kettering Cancer Center, New York, New York. [4]Weill Cornell/Rockefeller/Sloan Kettering Tri-Institutional MD-PhD Program, New York, New York. [5]Department of Computational and Systems Biology, Memorial Sloan Kettering Cancer Center, New York, New York. [6]Marron Cancer Metabolism Center, Memorial Sloan Kettering Cancer Center, New York, New York. [7]Immunology Program, Memorial Sloan Kettering Cancer Center, New York, New York. [8]Metabolomics Core Resource Library, New York University Langone Health, New York, New York. [9]Laboratory of Metabolic Regulation and Genetics, The Rockefeller University, New York, New York. [10]Department of Epidemiology-Biostatistics, Memorial Sloan Kettering Cancer Center, New York, New York. [11]Department of Surgery, Memorial Sloan Kettering Cancer Center, New York, New York. [12]Department of Pathology, Memorial Sloan Kettering Cancer Center, New York, New York.

Note: Supplementary data for this article are available at Cancer Discovery Online (http://cancerdiscovery.aacrjournals.org/).

Corresponding Author: Richard M. White, Memorial Sloan Kettering Cancer Center, 1275 York Avenue, MB 424, New York, NY 10065. Phone: 617-875-4590; Fax: 646-422-0231; E-mail: whiter@mskcc.org

doi: 10.1158/2159-8290.CD-17-1371

©2018 American Association for Cancer Research.

INTRODUCTION

The tumor microenvironment (TME) is increasingly recognized to play an important role in cancer initiation and progression. The variety of TME components acts in concert with genetic changes in tumor cells to allow for a dynamic response to novel environments during tumor progression and after exposure to drugs (1). The TME can also provide growth factors such as WNT ligands that drive tumor cell proliferation and invasion (2), making tumor–TME cross-talk an attractive therapeutic target.

In melanoma, components of the TME continue to be elucidated. Immune cells such as T cells are a major component of this environment, underscored by the recent success of immunomodulators such as anti-CTLA4 (3) and anti–PD-1 (4) molecules that have had dramatic efficacy in a significant number of patients with melanoma. A recent single-cell sequencing study demonstrated significant heterogeneity within the immune component of the TME (5), which may in part be related to the ability of immune cells such as macrophages to respond to lactate secreted from tumor cells (6). These observations may provide new opportunities for patient-specific immune therapies.

Melanomas arise from neural crest–derived melanocytes (7), which are anatomically located at the dermal–epidermal junction of the skin. During the early stages of melanoma, referred to as a Clark's level I tumor, melanoma cells interact with microenvironmental keratinocytes, which provide endothelins required for melanoma growth (8). As melanoma progresses, tumor cells enter a vertical growth phase and grow past the dermis into subcutaneous tissue, which is largely populated with adipocytes. These advanced, Clark's level V primary melanomas are at high risk of systemic metastasis. Melanoma cells also come into direct contact with adipocytes when they metastasize to secondary subcutaneous tissues or bone marrow (9), making these stromal cells a relevant component of both primary and metastatic microenvironments.

Despite long recognition that the subcutaneous tissue is composed of adipocytes, relatively little attention has been paid to the mechanistic interaction between melanoma cells and adipocytes. Cross-talk between the two cell types is likely: In mice, the adipocytic, subcutaneous tissue surrounding engrafted melanoma cells shows morphologic changes consistent with an activated cancer-associated adipocyte (10), likely due to lipolytic factors secreted from the melanoma

Downloaded from http://aacrjournals.org/cancerdiscovery/article-pdf/8/8/1006/1841481/1006.pdf by guest on 27 August 2022

cells (11). Moreover, adipocytes are lipid-rich, highly secretory cells that release lipids and a number of adipokines such as leptin that can drive melanoma growth through MAPK activation (12). A recent study demonstrated that adipocyte-derived exosomes carry proteins that drive fatty-acid oxidation in melanoma cells, suggesting they may influence melanoma cell metabolism (13). Here, we utilize a combination of mouse and zebrafish *in vivo* models and human patient-derived tissues to interrogate how stromal adipocytes can promote melanoma progression. We demonstrate that adipocytes donate high levels of fatty acids to melanoma cells, fueling proliferation and invasion. These adipocyte-derived fatty acids are transported into melanoma cells through the fatty acid transporter proteins (FATP), which are highly expressed in subsets of patients with melanoma and act to promote melanoma progression.

RESULTS

Advanced Melanomas Are in Direct Contact with Subcutaneous Adipocytes

Melanomas arise at the dermal–epidermal junction, where they initially expand in radial growth phase. During progression, these lesions extend down into the dermal tissue during vertical growth phase, and some lesions continue to grow into the subcutaneous tissues, where they are then classified as Clark's level V. Moreover, metastatic tumor cells can also reach subcutaneous tissues as in-transit metastases. Histologic examination of these advanced melanomas demonstrates that these tumors are encased by subcutaneous adipocytes present in the TME (Fig. 1A). We found that adipocytes directly adjacent to the tumor are diminished in size compared with those further away, consistent with tumor-induced lipolysis. Given the importance of adipocytes in other tumors, such as ovarian and breast cancers (14, 15), we reasoned that these subcutaneous adipocytes might promote melanoma growth and progression.

Adipocytes Increase Melanoma Cell Proliferation and Invasion

To assess the role of adipocytes in melanoma progression, we established an adipocyte–melanoma cell coculture system (Fig. 1B). We differentiated 3T3-L1 cells into adipocytes with mature lipid droplets and then grew human A375 or SKMel28 cells on top. We measured proliferation of melanoma cells with or without the adipocytes using pH3 staining (Fig. 1C). In both cell lines, we found a significant increase in melanoma cell growth when the cells were serum starved to remove other growth factors.

We next tested whether the adipocytes could also increase melanoma cell invasion, using several different assays. We found that adipocyte-conditioned media increased the ability of A375 melanoma cells to degrade a gelatin matrix in 2-D (Fig. 1D). We then utilized Transwell assays to measure if this increased the ability of the cells to invade through the membrane. We treated melanoma cells with adipocyte-conditioned media and found that this significantly increased the ability of the cells to invade into a collagen plug contained within the Transwell (Fig. 1E). Finally, we cocultured melanoma cells with or without adipocytes, FACS isolated the melanoma cells, and found that the adipocyte-exposed melanoma cells had a significantly increased ability to fully traverse a Transwell membrane that had been coated with Matrigel (Fig. 1F). Collectively, these data indicate that adipocytes can increase melanoma cells' aggressiveness.

Adipocytes Increase Melanoma Cell Lipid Content

Adipocytes could enact these changes in the melanoma cells either through adipokines (e.g., leptin) or via changes in melanoma cell lipid content. We performed RNA sequencing (RNA-seq) on A375 melanoma cells in the presence or absence of adipocytes and used Gene Set Enrichment Analysis to identify the most dysregulated pathways from the MSigDB database (ref. 16; Supplementary Fig. S1; Supplementary Table S1). This revealed a strong enrichment for defects in cholesterol homeostasis and fatty-acid metabolism. Based on these data and other studies showing that adipocytes can directly alter lipid content of tumor cells (14, 17), we therefore focused on lipid content in the melanoma cells.

To test whether adipocytes increase lipid content in melanoma cells, we utilized the coculture system above and measured melanoma cell lipid content. Human A375 or SKMel28 cells or zebrafish ZMEL1 cells were grown either in the presence or absence of adipocytes, FACS isolated, and lipid content was measured using the global lipid dye LipidToxRED. In all three cell lines, we found a significant increase in cytosolic lipids in the cocultured cells (Fig. 2A). We reasoned that this global increase in lipid content in the melanoma cells would lead to aberrant formation of lipid droplets in the cytosol. To assess this, we performed electron microscopy on A375 cells with or without adipocytes. We found a significant increase in both the number and size of the lipid droplets in the cocultured melanoma cells, consistent with the effects we see with LipidToxRED (Fig. 2B).

Adipocytes Directly Transfer Fatty Acids to Melanoma Cells

The above data indicate that the presence of adipocytes increases melanoma cell lipid content but does not indicate whether this is a result of direct transfer or an indirect effect of a secreted factor that triggers *de novo* fatty-acid synthesis in tumor cells. Because tumor-adjacent adipocytes are smaller than those far away (Fig. 1A), we tested whether they were direct donors to the melanoma cells by a lipid "pulse-chase" approach. 3T3-L1 adipocytes were loaded with BODIPY-labeled fatty acids. Labeled adipocytes were washed to remove excess lipids from the media, and melanoma cells were plated on top (Fig. 2C). Within 24 to 48 hours, we observed the BODIPY-labeled fatty acids within the cytosol of melanoma cells, demonstrating that lipid species originating from adipocytes could be transferred to melanoma cells. To determine whether direct melanoma cell–adipocyte contact was necessary for transfer, we also performed a second iteration of the experiment with adipocytes and melanoma cells separated by a Transwell membrane (Fig. 2D). Similar to what we observed when the cells were in direct contact, adipocyte-derived BODIPY-labeled fatty acids can be transferred into the melanoma cell (Fig. 2E), demonstrating that cell–cell contact is not necessary. This effect was seen for both C12 and C16 BODIPY-labeled fatty-acid chain lengths (Supplementary

Downloaded from http://aacrjournals.org/cancerdiscovery/article-pdf/8/8/1006/1841481/1006.pdf by guest on 27 August 2022

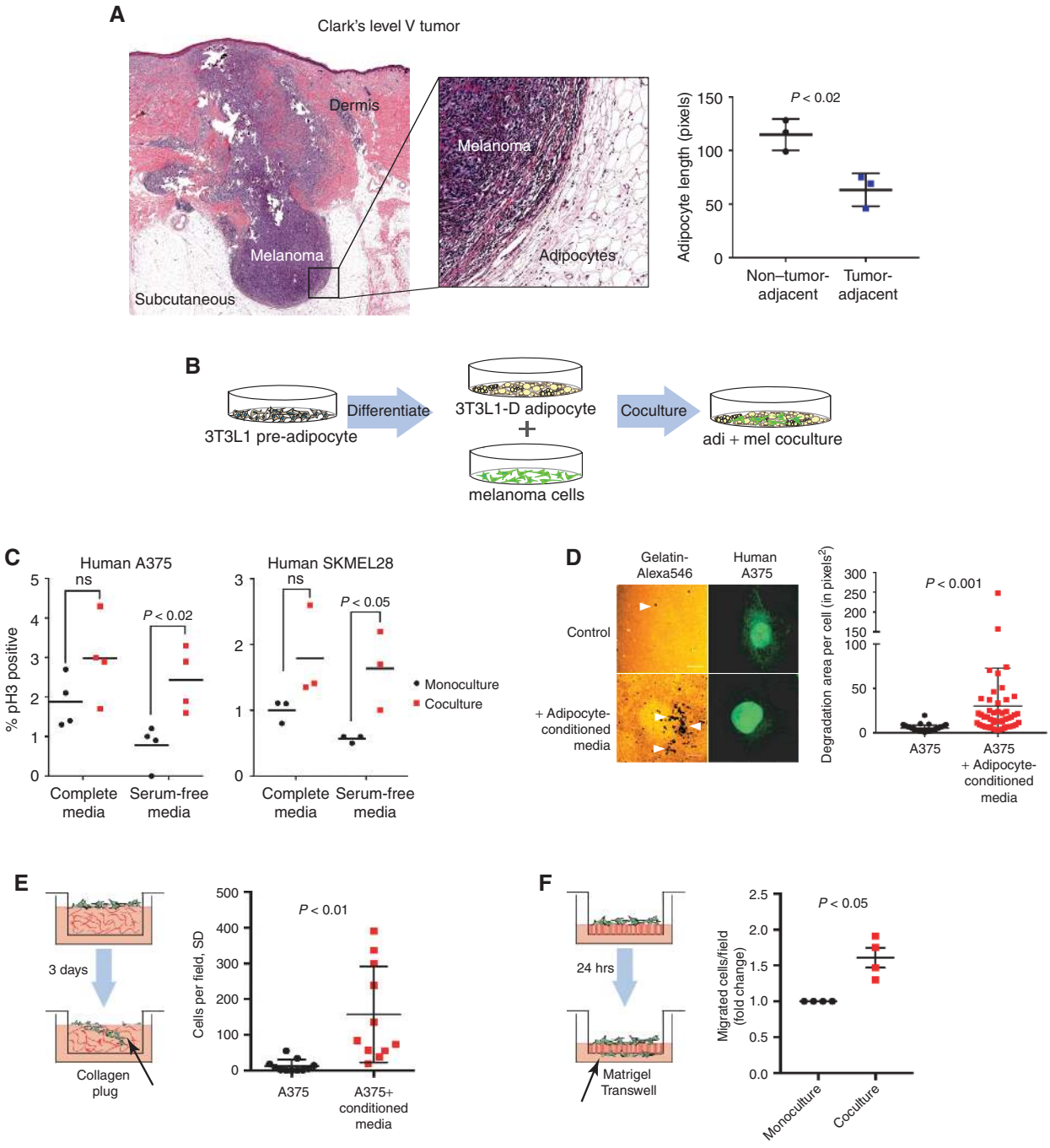

Figure 1. Tumor-adjacent adipocytes contribute to melanoma progression. **A,** Hematoxylin and eosin staining on a Clark's level V tumor. Vertical growth in the tumor (Mel) exposes melanoma cells to dermis as well as subcutaneous tissues, which is mainly composed of adipocytes. The graph shows quantification of maximum length of tumor-adjacent adipocytes and non–tumor-adjacent adipocytes. Each data point represents the average length of 10 to 15 tumor-adjacent and 10 to 15 non–tumor-adjacent adipocytes for 3 regions of interest in section. Error bars, SD. Two-tailed unpaired *t* test. **B,** Schematic showing the adipocyte–melanoma coculture system. **C,** Phosho-H3 staining in SKMel28-GFP and A375-GFP cells cocultured with 3T3L1 adipocytes for 24 hours. %pH3 was calculated by counting the number of $pH3^+$ nuclei over total number of GFP^+ cells/field. Each data point represents an average of >10 fields/condition. Two-tailed unpaired *t* test; $n \geq 3$ independent experiments. **D,** Gelatin degradation assay to measure invasive capacity of A375-GFP cells. A375-GFP cells were seeded on gelatin matrix and grown in control media or adipocyte-conditioned media for 24 hours. Degradation was calculated as the area of degraded gelatin as a proportion of the total cell area. Representative images are shown. Error bars, SD. *T* test with Welch correction; $n = 3$ independent experiments. Scale bars, 10 μm. Arrowheads indicate areas of degradation. **E,** A375-GFP were seeded on top of collagen-polymerized matrix and allowed to invade for 3 days. Quantification was done counting the number of cells invaded 30 to 60 μm into the collagen matrix per field (black arrow). Error bars, SD. Two-tailed unpaired *t* test with Welch correction; $n = 3$ independent experiments. **F,** Matrigel Transwell migration of FACS-isolated A375-GFP cells in monoculture or after coculture with 3T3L1 adipocytes for 7 days. Quantification was done counting the number of cells on the bottom side of the Transwell (black arrow) calculated as the fold change of number of cells in cocultured cells compared with monoculture controls. Each data point represents an average of ≥3 fields/condition per independent experiment. Two-tailed unpaired *t* test with Welch correction; $n = 4$ independent experiments.

Downloaded from http://aacrjournals.org/cancerdiscovery/article-pdf/8/8/1006/1841481/1006.pdf by guest on 27 August 2022

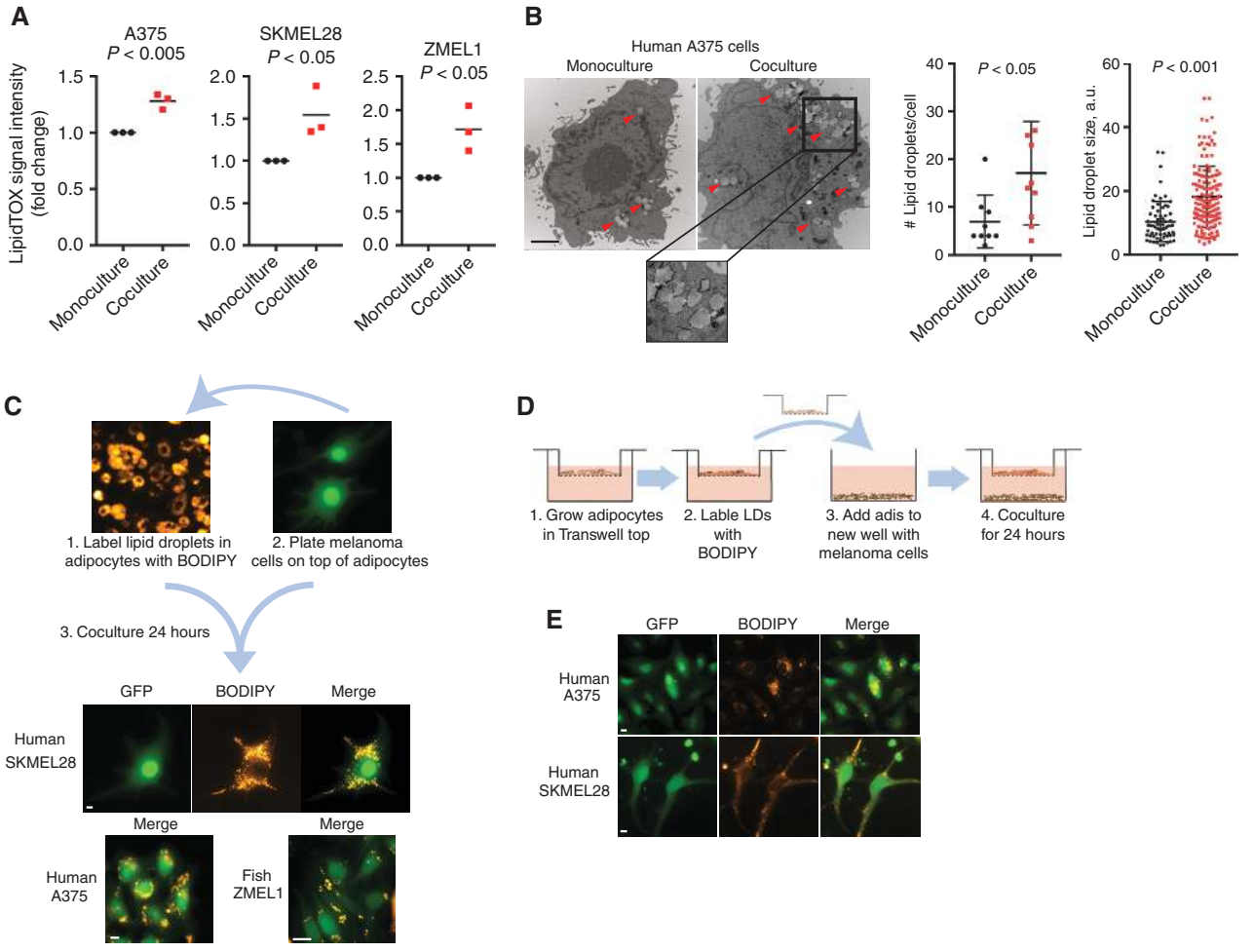

Figure 2. Adipocytes increase melanoma cell lipid content via adipocyte/melanoma lipid transfer. **A,** LipidTOX staining on ZMEL1-GFP, SKMel28-GFP, and A375-GFP cells that were cocultured with 3T3L1 adipocytes for 7 days and then FACS isolated. LipidTOX staining intensity was quantified and calculated as fold change of LipidTOX staining in cocultured cells compared with monoculture controls. Each data point represents an average of >10 fields/condition per independent experiment. Mean is shown. Two-tailed unpaired *t* test; $n = 3$ independent experiments. **B,** Transmission electron microscopy of A375-GFP cells FACS isolated after coculture with 3T3L1 adipocytes for 7 days compared with monoculture controls. Error bars, SD. Two-way unpaired *t* test with Welch correction, $n = 10$ cells/condition. Scale bar, 2 μm. Representative images are shown. **C,** Transfer of BODIPY fluorescent fatty acid from adipocytes to melanoma cells. 3T3L1 adipocytes were grown alone and lipid droplets were labeled with BODIPY. After washing away extracellular BODIPY, ZMEL1-GFP, SKMel28-GFP, or A375-GFP cells were plated on top and cocultured with BODIPY-labeled adipocytes for 24 hours and then fixed and imaged. Representative images shown; $n = 3$ independent experiments. Scale bars, 10 μm. **D,** 3T3L1 adipocytes were grown alone on the top portion of a Transwell and lipid droplets (LD) were labeled with BODIPY. After washing away extracellular BODIPY, Transwell inserts containing adipocytes were transferred to a new well containing ZMEL1-GFP, SKMel28-GFP, or A375-GFP cells. **E,** ZMEL1-GFP, SKMel28-GFP, or A375-GFP cells were cocultured for 24 hours and then fixed and imaged. Representative images shown; $n = 3$ independent experiments. Scale bars, 10 μm.

Fig. S2A). These data indicate that adipocytes can release fatty acids into the extracellular milieu, which can be taken up by nearby tumor cells, a phenomenon also observed in omental metastases in ovarian cancer (14).

Adipocytes Increase Dependency on Extrinsic Lipid Uptake in Melanoma Cells

These data raised the possibility that the adipocyte-derived lipids were affecting melanoma cell metabolism. To test this, we used the Seahorse assay to measure both mitochondrial oxygen consumption (OCR) and extracellular acidification rate (ECAR) in melanoma cells in monoculture or after coculture with adipocytes. Although ECAR did not change significantly between each condition (Supplementary Fig. S3), indicating no change in rates of glycolysis, cocultured melanoma cells had significantly increased OCR (Fig. 3A). This increase could be suppressed by etomoxir, an inhibitor of carnitine palmitoyl transferase (CPT1), which is necessary for a critical step in β-oxidation of fatty acids. Whereas the monocultured cells saw a small decrease in OCR after the addition of etomoxir, cocultured cells dramatically reduced OCR. Because CPT1 is an important first step in β-oxidation, this decrease in OCR is consistent with the idea that the cocultured cells can utilize the adipocyte-derived lipids for fatty-acid oxidation (Fig. 3B). We next tested whether these adipocyte-derived lipids made the melanoma cells less

Downloaded from http://aacrjournals.org/cancerdiscovery/article-pdf/8/8/1006/1841481/1006.pdf by guest on 27 August 2022

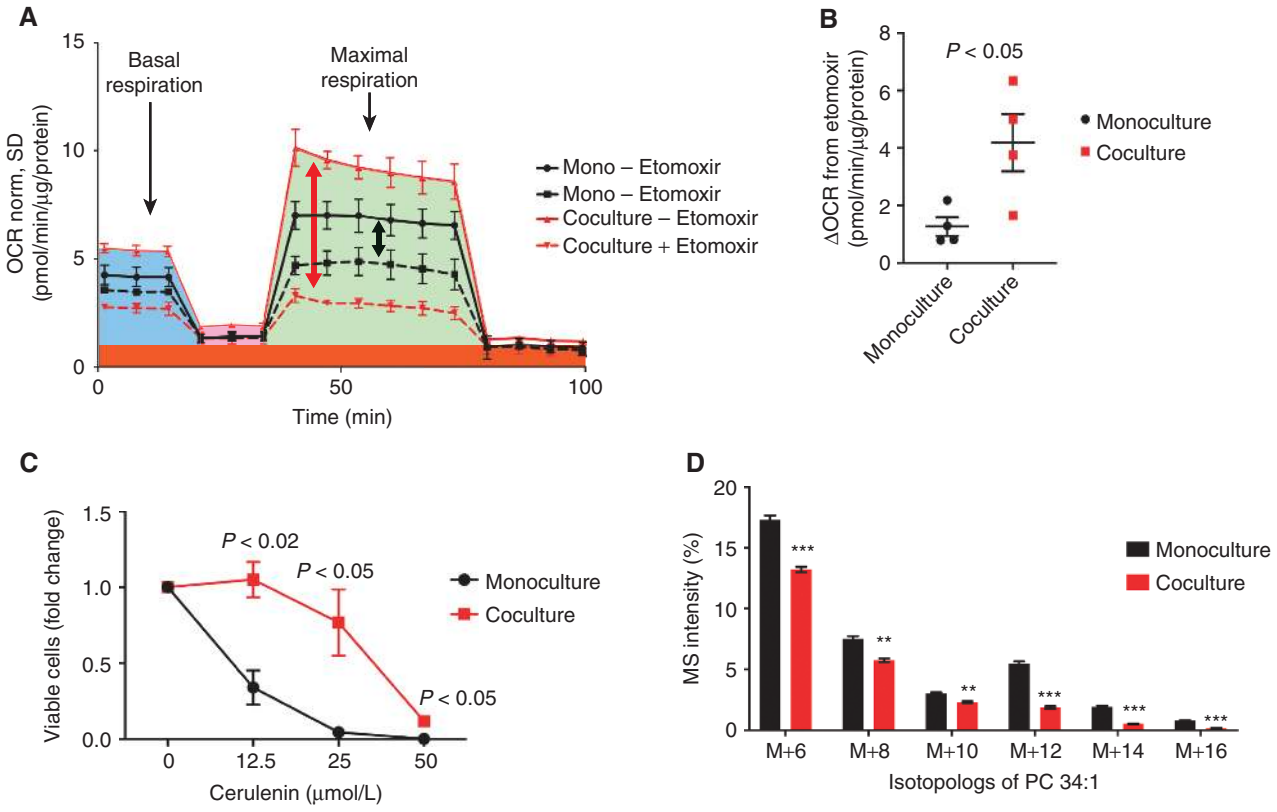

Figure 3. Adipocytes alter melanoma cell fatty-acid metabolism. **A,** Mitochondrial respiration of FACS-isolated A375-GFP cells in monoculture or after coculture with 3T3L1 adipocytes for 7 days with or without pretreatment with the CPT1 inhibitor etomoxir. OCR was measured under basal conditions followed by the sequential addition of oligomycin (1 µmol/L), FCCP (2 µmol/L), 0.5 µmol/L rotenone/antimycin A. Representative experiment is shown of 4 independent experiments. Error bars, SD. **B,** Quantification of change (Δ) in maximal OCR with treatment of 40 µmol/L etomoxir in monoculture and cocultured A375-GFP cells. Two-tailed unpaired *t* test with Welch correction; $n = 4$ independent experiments. **C,** Quantification of A375-GFP cells in monoculture or in coculture with adipocytes with or without various doses of the FASN inhibitor cerulenin, calculated as fold change compared with vehicle controls. Two-tailed unpaired *t* test with Welch correction; $n = 4$ independent experiments. **D,** Relative abundance of ^{13}C-labeled isotopologs of PC34:1 were quantified for A375 cells in monoculture or after coculture with adipocytes for 7 days and treated with ^{13}C-acetate for 24 hours. Multiple two-tailed *t* test with the Holm–Sidak test for multiple comparisons. **, $P < 0.005$; ***, $P < 0.001$.

dependent upon *de novo* lipogenesis by testing the sensitivity to the FASN inhibitor cerulenin. Whereas the monocultured cells had a significant decrease in cell viability from the FASN inhibitor, the cocultured cells were markedly protected from this effect (Fig. 3C). Finally, we reasoned that cocultured cells would have decreased rates of *de novo* lipid synthesis, as they were already taking up extrinsic lipids. We tested this by feeding melanoma cells ^{13}C-labelled acetate and measuring incorporation into newly synthesized lipids via LC/MS. This showed a significant decrease in *de novo* fatty-acid synthesis in the cocultured cells (Fig. 3D). Taken together, these data demonstrate that adipocyte-derived lipids can be utilized in the β-oxidation pathway and decrease the dependence on *de novo* lipogenesis.

Adipocytes Increase Melanoma Cell Lipid Content *In Vivo*

We next wanted to test whether the increased lipid content from adipocytes occurred *in vivo*. We first examined a series of human subcutaneous metastases and tumors from patient-derived xenografts (PDX) and stained them for OilRedO, a commonly used lipid dye in human samples (Fig. 4A; Supplementary Fig. S4). In 3 of 5 patient biopsy samples and 4 of 4 PDXs, we found significant evidence of lipid accumulation in the cytosol of tumor cells that are directly adjacent to adipocytes (see additional data in Fig. 6 related to the mechanism of this lipid accumulation).

We next turned to an animal model of this process. Our lab has previously developed a *BRAF*^{V600E}-driven transgenic zebrafish model of melanoma that closely recapitulates the human disease (18, 19). From this model, we also developed a GFP-labeled melanoma cell line called ZMEL1, which can be used for transplantation studies. We wished to determine if transplantation of ZMEL1 cells into adipocytes would recapitulate the increases in lipid content that we had observed *in vitro* (20). We first identified the location of the zebrafish adipocyte fat pad using a *plin2-tdTomato* transgenic line, which showed a depot of subcutaneous fat in the ventral and dorsal skin (Fig. 4B). Based on this anatomy, we transplanted ZMEL1-GFP melanoma cells directly into the ventral subcutaneous fat pad of the fish and then stained with BODIPY-RED to visualize lipids. This imaging revealed clear

Downloaded from http://aacrjournals.org/cancerdiscovery/article-pdf/8/8/1006/1841481/1006.pdf by guest on 27 August 2022

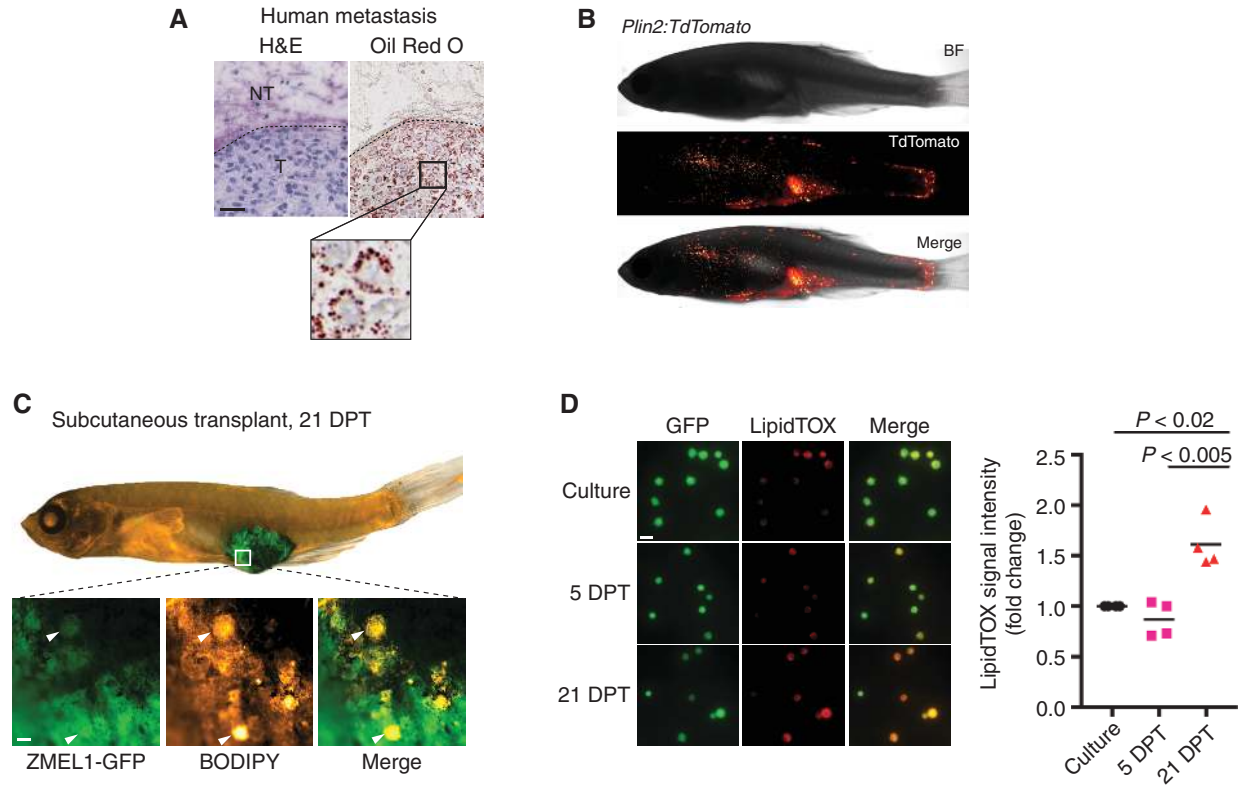

Figure 4. Adipocytes increase melanoma cell lipid content *in vivo*. **A,** Patient-derived subcutaneous acral melanoma metastases stained with hematoxylin and eosin (H&E) and Oil Red O. Scale bar, 100 μm. T, tumor; NT, nontumor. **B,** Casper transparent adult zebrafish with adipocyte-specific TdTomato expression driven by the *Plin2* promoter. **C,** Adult Casper at 21 DPT with ZMEL1-GFP cells. Fish is stained with BODIPY 558/568 to visualize lipids. Insets show BODIPY-labeled GFP$^+$ cells, revealing a subset of tumor cells that are lipid-laden. Representative images are shown. Double-positive cells (arrowheads) were observed in 16 of 21 transplanted fish. Scale bar, 50 μm. **D,** ZMEL1-GFP cells were transplanted subcutaneously into adult Casper fish until 5 or 21 DPT and then FACS isolated and stained for total lipid content with LipidTOX. LipidTOX staining intensity was quantified calculated as fold change of LipidTOX staining in transplanted ZMEL1 cells compared with cultured parental controls. Each data point represents an average of >10 fields/condition per independent experiment. Mean is shown. Two-tailed unpaired *t* test; $n = 4$ independent experiments. Scale bar, 20 μm.

evidence of lipid-laden melanoma cells (Fig. 4C) in 76% of the fish, an effect that was not seen when the cells were next to adipocyte-free areas of the fish (Supplementary Fig. S5). To more precisely quantify this effect, we FACS isolated the GFP$^+$ melanoma cells at 21 days after transplant (DPT) and analyzed them by *ex vivo* lipid analysis using LipidToxRED staining. Analogous to what we saw *in vitro*, by 21 DPT, we saw a significant increase in global lipid content in the ZMEL1 melanoma cells compared with cells growing *in vitro* or after a short 5-day period of *in vivo* growth (Fig. 4D).

Subcutaneous Metastases Grow Next to Adipocytes and Dysregulate Lipid Genes

Given the changes in tumor cell metabolism we observed in the melanoma–adipocyte cocultured cells and the parallel increases in lipid content in transplanted tumor cells, we next wanted to determine whether subcutaneous metastases showed changes in lipid metabolism. We utilized a previously developed zebrafish metastasis assay in which the ZMEL1-GFP cells can be injected either into the skin or directly into vasculature, and metastatic engraftment to secondary subcutaneous sites can be read out at 21 days. We sectioned recipient fish and found that 57% of the metastases developed directly adjacent to endogenous adipocytes (Fig. 5A). We isolated the subcutaneous metastatic cells by FACS and performed RNA-seq analysis on tumor cells that were growing next to adipocytes (Fig. 5B; Supplementary Table S2). Ingenuity Pathway Analysis showed that of the top dysregulated pathways, 3 of 7 were centered on abnormalities of adipogenesis, fatty-acid synthesis, or cholesterol synthesis (Fig. 5C). Moreover, most *de novo* lipogenesis genes were strongly downregulated due to feedback inhibition, as expected for cells avidly taking up extrinsic lipids (Fig. 5D) and consistent with our *in vitro* data using the FASN inhibitor and ^{13}C incorporation (Fig. 3C and D). Taken together, these data confirm that the effects we observed *in vitro* are conserved *in vivo*.

Global Lipidomics Demonstrates That Long-Chain Fatty Acids Are Transferred to Melanoma Cells

The above data suggested that melanoma cells can take up lipids from adjacent adipocytes both *in vitro* and *in vivo*. To directly assess the lipid species donated by adipocytes to melanoma cells, we performed global lipidomic profiling of melanoma cells in both the *in vitro* and *in vivo* situations. For the *in vitro* experiments, we cocultured A375 or ZMEL1 melanoma cells with or without 3T3L1 adipocytes, as above. We

Downloaded from http://aacrjournals.org/cancerdiscovery/article-pdf/8/8/1006/1841481/1006.pdf by guest on 27 August 2022

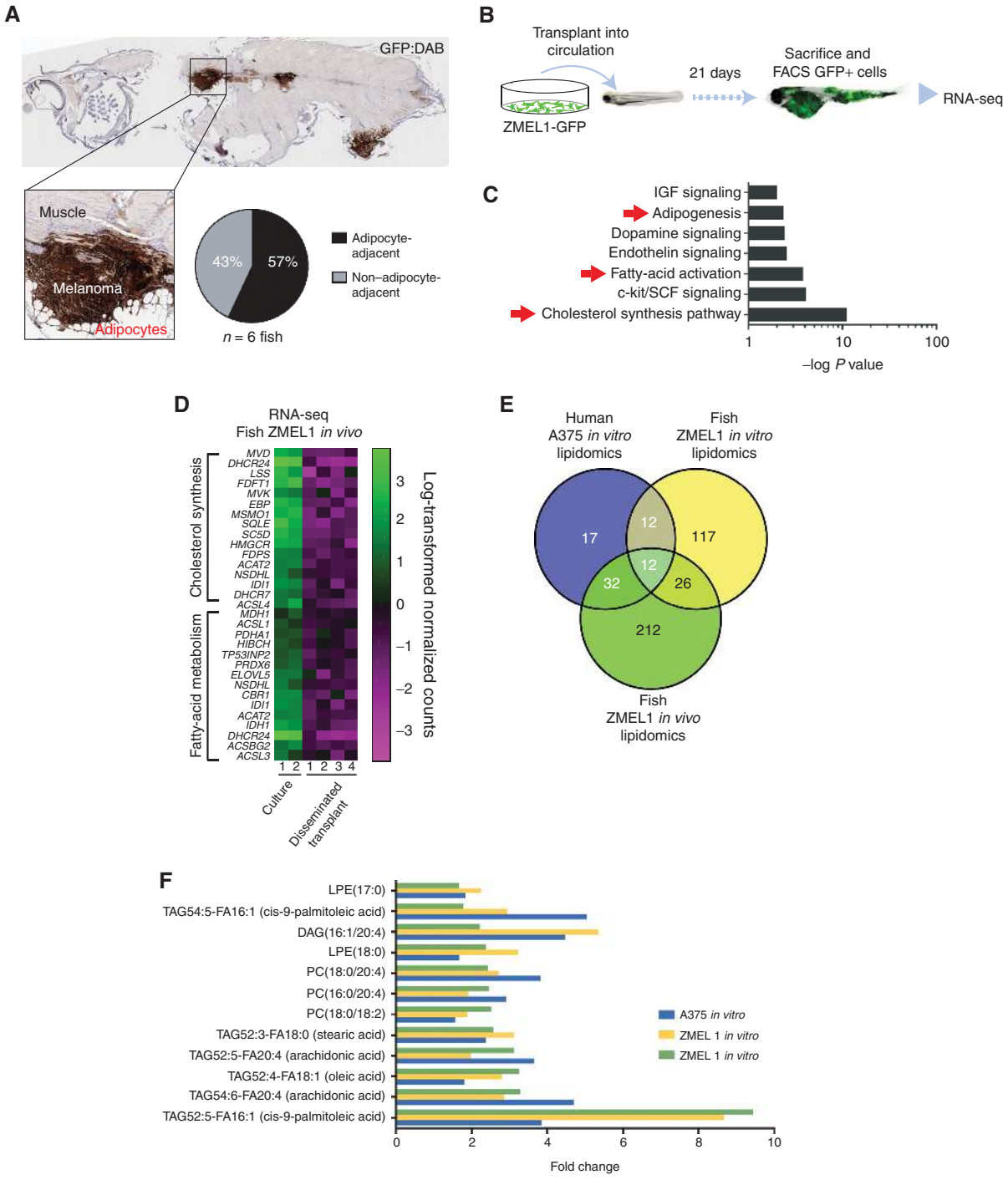

Figure 5. Subcutaneous metastases grow next to adipocytes and dysregulate lipid genes. **A,** GFP staining of a Casper transplanted fish at 18 DPT showing adipocyte-adjacent and non–adipocyte-adjacent metastases. For $n = 6$ fish, total number of metastases and number of metastases next to adipocytes were quantified. **B,** Schematic of evaluating melanoma metastasis using transplantation into zebrafish larvae. ZMEL1-GFP cells were transplanted into the vasculature of a fish at 2 days after fertilization. At 21 DPT, when fish had widespread tumor dissemination, GFP$^+$ cells were isolated by FACS. Parental ZMEL1-GFP cells maintained in culture were also subject to FACS sorting, and gene expression profiling was performed on the two cell populations. **C,** Ingenuity Pathway Analysis of ZMEL1-GFP cells after metastatic dissemination suggests seven pathways that could mediate microenvironmental effects on melanoma growth. *P* values indicate estimated likelihood that the indicated pathway is altered in the RNA-seq data set. **D,** Heat map of RNA-seq expression of genes with significant differential expression between zebrafish ZMEL1 cells grown either in culture or in disseminated transplants in zebrafish, showing downregulated genes that are typical SREBP targets. **E,** Common lipid species that are increased in human A375 (blue) or zebrafish ZMEL1 (yellow) cells grown in coculture with adipocytes (compared with monoculture) and from zebrafish ZMEL1 cells grown in subcutaneous transplants in zebrafish (compared with parental cells in culture; green). **F,** 12 lipid species that commonly increased between *in vitro* human A375 and zebrafish ZMEL1 cells cocultured with adipocytes and from ZMEL1 cells grown in subcutaneous transplants. Two-tailed unpaired *t* test; $n = 3$, $P < 0.05$.

Downloaded from http://aacrjournals.org/cancerdiscovery/article-pdf/8/8/1006/1841481/1006.pdf by guest on 27 August 2022

then FACS isolated the melanoma cells, along with control melanoma cells that were maintained in monoculture. For the *in vivo* experiments, we transplanted ZMEL1 cells into the subcutaneous fat pad, as above, and FACS isolated the melanoma cells 21 DPT. Mass spectrometry–based lipid profiling of 1,088 individual lipid species was performed on these *in vitro* and *in vivo* tumor cell samples (Supplementary Fig. S6A; Supplementary Tables S3–S5). We calculated the fold change of each species compared with the monocultured cells and identified the lipid species that were increased across the *in vitro* and *in vivo* samples (Fig. 5E). Overall, the most significantly increased lipids were long-chain fatty acids, including both saturated (e.g., stearic acid) and unsaturated (e.g., oleic acid) species (Fig. 5F). To confirm the physiologic relevance of these lipids, we then determined whether these fatty acids were sufficient to promote melanoma growth even in the absence of adipocytes. We used a chemically defined lipid reagent (CDL) that contains a mixture of saturated and unsaturated fatty acids, and measured growth of A375 melanoma cells in complete media and serum-free media. In both conditions, the CDL mixture promoted melanoma growth across a range of time points (Supplementary Fig. S6B).

Long-Chain Fatty Acids Are Taken Up by FATP/SLC27A Proteins on the Melanoma Cells

Long-chain fatty acids such as stearic and oleic acid require active transport to enter the cytosol. In cells such as liver and brain, this uptake is mediated by the FATP family of lipid transporters (21, 22). Humans have 6 highly related FATP/SLC27A proteins, referred to as FATP1–6. To determine which was most relevant to melanoma, we examined the expression of this family of proteins using data from the Cancer Cell Line Encyclopedia and the Oncomine database (Supplementary Fig. S7A). This revealed a statistically significant enrichment of *FATP1/SLC27A1* in melanoma compared with all other cancer types, and we found that in stage IV patients, higher mRNA levels correlated with worse survival (ref. 23; Supplementary Fig. S7B). This prompted us to examine protein expression of FATP1 in human patient biopsies as well. Consistent with the cell line data, we find that 44% of patients overexpress FATP1 specifically in the tumor cell compartment (Fig. 6A; Supplementary Fig. S4). To determine if there was a relationship between FATP1 expression and lipid uptake, we stained a series of freshly isolated tumors from both primary and metastatic sites (subcutaneous, lymph nodes, and brain) for both FATP1 and lipids using Oil Red O, which revealed a strong positive correlation ($r^2 = 0.61$) for FATP1 versus Oil Red O staining (Fig. 6B). These data are in line with the known ability of FATP1 in mediating uptake of long-chain fatty acids.

To functionally assess whether FATP1 is capable of mediating lipid uptake into melanoma cells, we overexpressed FATP1 in A375 human melanoma cells and found that it significantly increased fatty-acid uptake (Fig. 6C). Conversely, fatty-acid uptake was impaired when FATP1 expression was abrogated with CRISPR/Cas9 (Fig. 6D; Supplementary Fig. S8A). To test the importance of FATP1 *in vivo*, we utilized both zebrafish transgenesis and mouse xenografts. We generated transgenic zebrafish in which the *BRAF*^{V600E} gene is expressed with or without concomitant overexpression of *FATP1*. To do this, we utilized the previously described MiniCoopR system, a mosaic transgenic system in which any cargo gene of interest (e.g., *FATP1*) can be easily inserted and expressed coordinately with *BRAF*^{V600E} under the melanocyte-specific *mitfa* promoter (24). This ensures melanocyte-specific BRAF^{V600E} and FATP1 expression, limiting off-target effects in other cell types. We then followed a cohort of *BRAF*^{V600E} versus *BRAF*^{V600E}*;FATP1* animals for a period of 4 months. In this time frame, only a small number of *BRAF*^{V600E}-alone animals developed melanomas (4%). In contrast, we saw a marked acceleration of melanoma development in the *BRAF*^{V600E}*;FATP1* animals (30%; Fig. 6E). For a subset of animals that developed tumors, we stained the fish with BODIPY-RED to visualize lipid content. Whereas *BRAF*^{V600E} alone had only scant amounts of lipid staining, nearly the entire *BRAF*^{V600E}*;FATP1* tumor stained strongly with BODIPY-RED, consistent with a lipid-filled tumor, as expected (Fig. 6F).

Next, we wanted to confirm if this effect was conserved in mouse xenograft studies. We stably infected *BRAF*^{V600E}-mutant A375 melanoma cells with either an mCherry or *FATP1*-mCherry cassette using lentiviral transduction. We transplanted these cells into the subcutaneous tissues of recipient nude mice and followed tumor growth over 28 days. Similar to what we observed in the zebrafish studies, FATP1 overexpression increases tumor growth in the mouse (Fig. 6G). Taken together, these data indicate that FATP1 acts to promote melanoma growth in the context of BRAF^{V600E}.

FATP Blockade Inhibits Melanoma Growth

These data raised the possibility that pharmacologic blockade of FATP proteins might have therapeutic utility in melanoma. We therefore wished to test this both *in vitro* and *in vivo*. Recent work has identified a small-molecule FATP inhibitor called Lipofermata/CB16.2 (25), which was initially isolated as a FATP2 inhibitor that could be used for the treatment of fatty liver disease (26). Given the similarities between FATP1 and FATP2, our data suggested that this molecule might be repurposed for use in melanoma. To test this, we first determined whether Lipofermata could also block FATP1 by measuring lipid uptake in FATP1-overexpressing or knockout cells. Lipofermata dose-dependently inhibited lipid transport in A375 cells overexpressing FATP1, an effect that was diminished in the CRISPR knockout cells (Supplementary Fig. S9). Next, we tested the effects of Lipofermata on A375 cells expressing endogenous levels of FATP1, and found it inhibited fatty-acid uptake in a dose-dependent manner (Fig. 7A). This effect did not occur using a molecule that is structurally similar to Lipofermata (CB16.6) but has previously been shown not to block lipid uptake (Supplementary Fig. S10A) in CaCO2 and HepG2 cells (26). Next, we tested Lipofermata using the lipid pulse-chase experiment described above. We differentiated 3T3-L1 cells into adipocytes, loaded them with BODIPY-RED fatty acids, and then plated melanoma cells onto these in the presence or absence of Lipofermata. This revealed a strong abrogation of lipid transfer from the adipocyte to the melanoma cell (Fig. 7B). We next measured proliferation and found a dose-dependent decrease in proliferation with Lipofermata treatment in multiple melanoma cell lines that was not observed with cells treated with the inactive compound CB16.6 (Fig. 7C; Supplementary Fig. S10B). This

Downloaded from http://aacrjournals.org/cancerdiscovery/article-pdf/8/8/1006/1841481/1006.pdf by guest on 27 August 2022

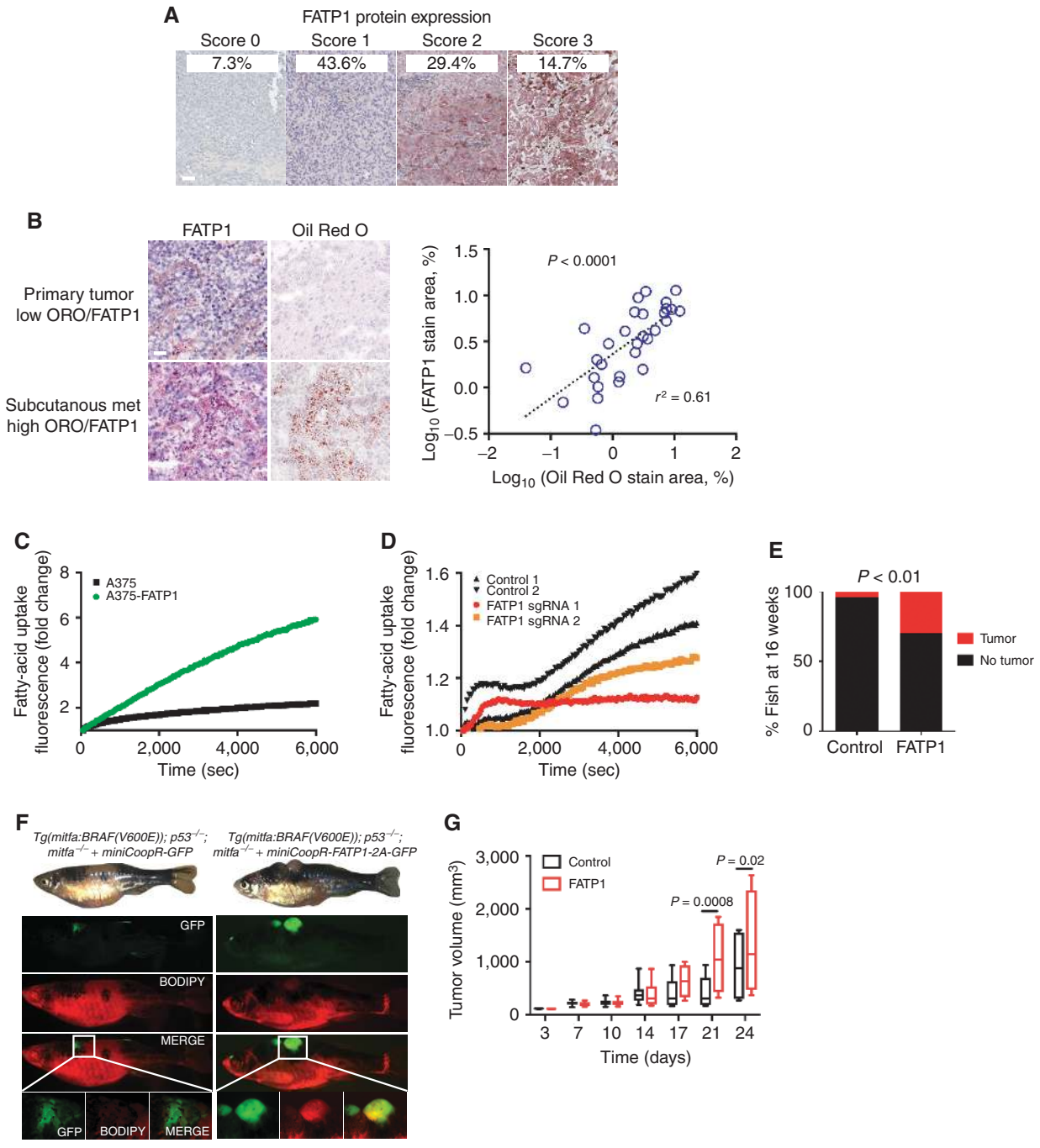

Figure 6. Aberrantly expressed FATP1 mediates lipid uptake in human melanomas. **A,** Immunohistochemistry images of endogenous FATP1 in a panel of 105 clinically defined human melanoma tumor samples. Representative images are shown. Score 0 represents no FATP staining, scores 1 and 2 represent low–medium FATP staining, and score 3 represents high FATP staining. Scale bar, 100 μm. **B,** Immunohistochemistry images of low FATP1 expression and Oil Red O (ORO) staining in a primary tumor and high FATP1 expression and ORO staining in a subcutaneous metastasis. Graph shows correlation of FATP1 expression and ORO staining in 7 patient samples consisting of one primary tumor and six subcutaneous and nonsubcutaneous metastases. r^2 based on Spearman rank-order correlation coefficient. Scale bar, 100 μm. **C,** QBT real-time lipid uptake in A375-overexpressing FATP1 compared with control cells. Graph represents mean from 3 independent experiments. Area under the curve (AUC) was calculated for each curve, and differences were compared by 95% confidence intervals. **D,** QBT timed lipid uptake in A375 FATP1 CRISPR knockout cells compared with control cells. Graph represents mean from 3 independent experiments. AUC was calculated for each curve, and differences were compared by 95% confidence intervals. sgRNA 1 and 2 had 73% and 55% mutant reads, respectively, validated via sequencing. **E,** MiniCoopR-*EGFP* or MiniCoopR-*FATP1* was injected into *Trp53/BRAF/Nacre* embryos. Percentages indicate melanoma incidence at 16 weeks of age, and statistical differences in tumor incidence were quantified with Chi-square test. **F,** MiniCoopR-*EGFP* or MiniCoopR-*FATP1* fish were stained with BODIPY-RED to visualize lipid burden in GFP+ tumor regions. Representative images are shown. **G,** Tumor volumes over time of nude mice harboring A375-mCherry or A375-FATP1-mCherry subcutaneously xenografted tumors. Error bars, SD. $n = 5$ individual xenograft mice per group.

Downloaded from http://aacrjournals.org/cancerdiscovery/article-pdf/8/8/1006/1841481/1006.pdf by guest on 27 August 2022

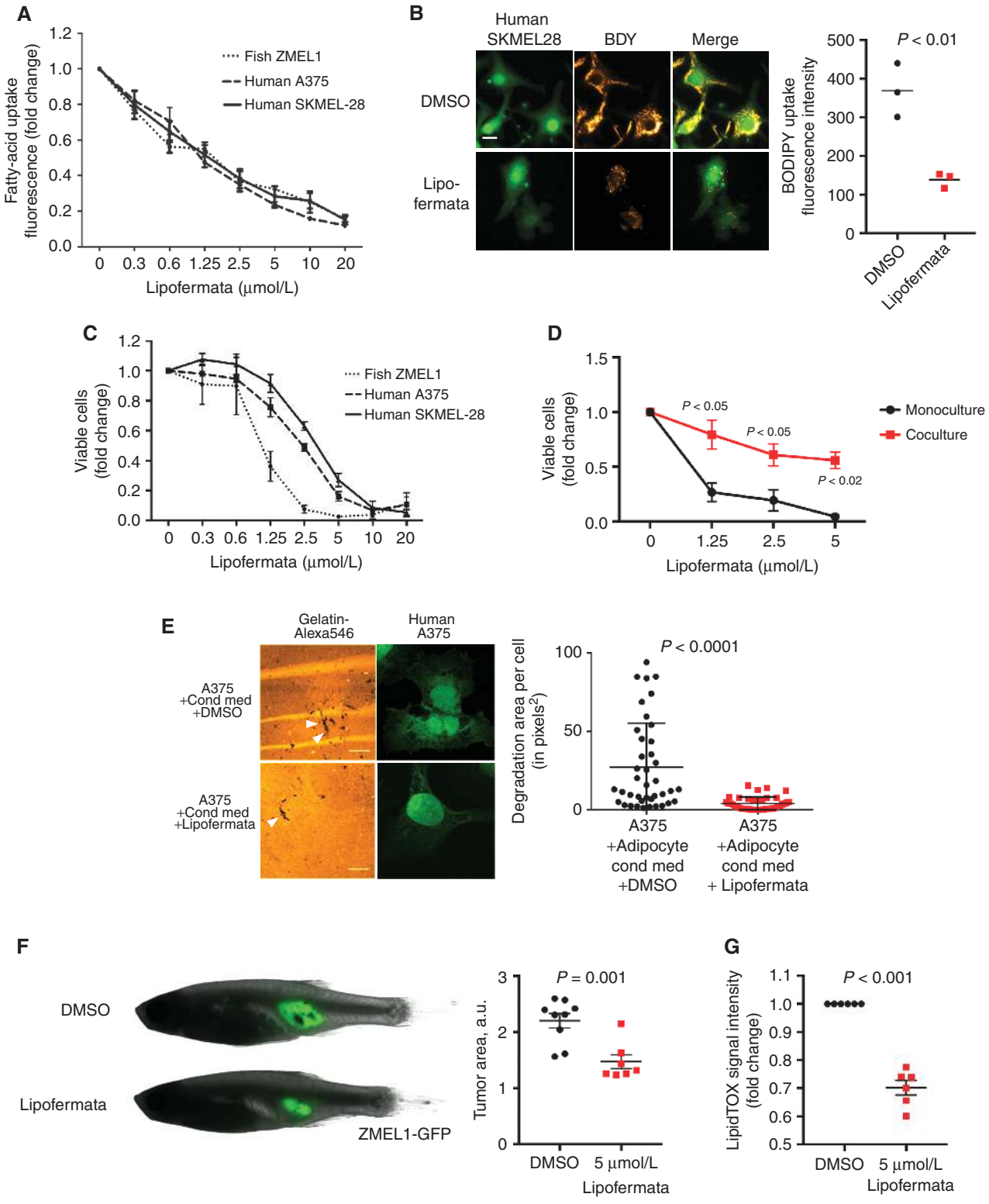

Downloaded from http://aacrjournals.org/cancerdiscovery/article-pdf/8/8/1006/1841481/1006.pdf by guest on 27 August 2022

effect on proliferation was diminished in melanoma cells that had previously been cocultured with adipocytes, as they have already taken up extrinsic lipids in that setting (Fig. 7D). We measured the invasive capacities of melanoma cells with the gelatin degradation assay after FATP inhibition with Lipofermata. At concentrations that did not cause cell death (Supplementary Fig. S11), Lipofermata abrogated the invasive phenotype we previously observed in tumor cells treated with adipocyte-conditioned medium (Fig. 7E).

Finally, we tested Lipofermata *in vivo*. One major limitation of this approach is the short half-life of Lipofermata *in vivo* (26), likely due to rapid liver clearance. Therefore, to take this into account, we wished to apply the drug directly to the tumor *in vivo*, bypassing liver clearance. Using our zebrafish transplant assay, we transplanted ZMEL1-GFP cells into the subcutaneous fat pad as above, waited for the tumor to engraft, and then injected Lipofermata into the tumor bed over the next 5 days. We measured tumor area by GFP expression and found that Lipofermata caused a significant decrease in melanoma cell growth (Fig. 7F). This was accompanied by a significant decrease in lipid content in the drug-treated tumors as measured by LipidTox staining (Fig. 7G). We also tested Lipofermata in mouse xenografts using systemic administration but did not see significant effects (on either tumor volume or animal weight) because of its short-half life, precluding us from adequately assessing its efficacy in this setting. This indicates that although further work will be needed to optimize Lipofermata or related molecules for clinical use, our data from the *in vitro* and zebrafish studies are consistent with the importance of FATP proteins as a viable target aimed at adipocyte–melanoma cross-talk.

DISCUSSION

It has long been posited that tumor cells will optimally grow when surrounded by environments that enhance their ability to proliferate and avoid cell death, often referred to as the "seed and soil" hypothesis (27, 28). *In vivo*, this soil is provided by the TME, which is now appreciated to play a central role in metastasis and drug resistance (29). The cell types and factors that are important within the TME continue to be elucidated, and our data are consistent with emerging data from other cancer types, demonstrating the contribution of stromal adipocytes to tumor progression. In ovarian (14), breast (30, 31), and other cancers (32, 33) known to initiate in or metastasize to adipose tissue, adipocyte-derived lipids are recognized as potent energy sources that support tumor cell metabolism and growth (14, 34). Aside from this energetic effect, adipocyte-secreted adipokines stimulate angiogenesis and proliferation (35). In cutaneous melanoma, progression is marked by the vertical growth phase of the tumor, when cells drive down from the dermal–epidermal junction into subcutaneous tissue. Although subcutaneous tissues are well known to be enriched for adipocytes, adipocyte function in melanoma has remained minimally explored, with only a few studies directly addressing its role in metabolism, invasion, or drug resistance (13, 36, 37). In this work, we define these subcutaneous adipocytes as a potent source of lipids that drive melanoma progression.

In many tumors, lipids are provided via *de novo* lipogenesis, making lipid synthetic pathways such as FASN potential therapeutic targets (38). In contrast, we find that melanoma cells take up lipids from the subcutaneous adipocytes, bypass the need for *de novo* synthesis, and in fact turn off the enzymes needed for lipogenesis. Our data show that after exposure to adipocytes, melanoma cells can take up extrinsic lipids and become less dependent upon FASN-mediated *de novo* lipogenesis, implying that lipid pathways outside of lipogenesis may be necessary in melanoma. Our work suggests that interrupting the mechanisms of lipid uptake from microenvironmental adipocytes may offer one such route. In support of this idea, recent work has demonstrated that CD36, a scavenger receptor that can transport fatty acids and other molecules, is a relevant therapeutic target in metastasis-initiating cells (39). Because CD36 binds multiple ligands, it largely relies on cotransporters to mediate specific transport of fatty acids into cells, which are most typically members of the FATP/SLC27A family (21). We have demonstrated that melanomas express FATPs and that these proteins mediate delivery of lipids from adipocytes to melanoma cells. Thus, although CD36 may selectively mark a subset of metastasis-initiating cells, melanoma cells that coexpress CD36 along with FATP proteins may be more broadly involved in both growth and invasive properties. Supporting this notion, we find a strong positive correlation between FATP1 expression and lipid content in the tumor cells, suggesting that melanomas expressing especially high levels of FATP proteins may be most responsive to nearby adipocytes. Inhibition of FATP

Downloaded from http://aacrjournals.org/cancerdiscovery/article-pdf/8/8/1006/1841481/1006.pdf by guest on 27 August 2022

Figure 7. FATP blockade inhibits melanoma growth and invasion. **A,** Lipid uptake assay in A375, SKMel28, and ZMEL1 cells treated with Lipofermata represented as mean fold change over control. $n = 3$ independent experiments. **B,** Representative images of lipid transfer assay in the presence of Lipofermata. 3T3L1 adipocytes were maintained on the top chamber of a Transwell insert, and intracellular lipid droplets were labeled with BODIPY. After labeling, Transwell inserts with 3T3L1 adipocytes were moved to a well containing melanoma cells and 2.5 μmol/L Lipofermata for 24 hours. Each data point represents an average of >10 fields/condition per experiment. Two-tailed unpaired *t* test; $n = 3$ independent experiments. Scale bar, 10 μm. **C,** CellTiter-Glo assay for cell viability on A375, SKMel28, and ZMEL1 cells treated with varying doses of Lipofermata for 72 hours. Data, mean fold change; $n = 3$ independent experiments. **D,** Quantification of A375-GFP cells in monoculture or in coculture with adipocytes with or without Lipofermata, calculated as fold change compared with vehicle controls. Two-tailed unpaired *t* test with Welch correction; $n = 3$ independent experiments. **E,** Gelatin degradation assay to measure invasive capacity of A375-GFP cells cultivated in adipocyte-conditioned media treated with DMSO or 1.5 μmol/L Lipofermata. Representative images are shown. Error bars, SD. *T* test with Welch correction; $n = 3$ independent experiments. Scale bars, 10 μm. Arrowheads indicate degradation. **F,** Representative images of tumor burden measured by GFP^+ tumor area after daily injection of 5 μmol/L Lipofermata into adult Casper fish transplanted with 3×10^6 ZMEL1-GFP cells. Tumor area for each fish, represented as one data point, is shown. Two-tailed unpaired *t* test; $n = 7$ Lipofermata-treated fish and $n = 9$ DMSO-treated fish. **G,** LipidTOX staining of GFP^+ tumor after daily injection of 5 μmol/L Lipofermata into adult Casper fish transplanted with 3×10^6 ZMEL1-GFP cells. LipidTOX intensity was quantified and calculated as fold change of staining Lipofermata-treated tumors compared with DMSO controls. Each data point represents an average of >10 fields/condition per fish. Error bars, SEM. Mean is shown. Two-tailed unpaired *t* test; $n = 6$ Lipofermata-treated fish and $n = 6$ DMSO-treated fish.

proteins with Lipofermata abrogates lipid transfer into melanoma cells. The relatively short half-life of this compound makes it more of a tool rather than a drug, but the FATP proteins may represent a future pharmacologic strategy to exploit the dependence of melanoma on adipocyte–melanoma cross-talk during tumor progression.

Lipids can exert complex effects on tumor cell behavior due to their structural diversity (40). Some lipids such as long-chain fatty acids can be used directly in beta-oxidation and act as a source of ATP for cell growth and metabolism (13). At the same time, high levels of lipids, especially saturated fatty acids, can lead to significant lipotoxicity (41). This can be due to increased levels of reactive oxygen species or induction of an endoplasmic reticulum stress response (42, 43). In addition to these metabolic functions, some lipids such as phospholipids and cholesterol can play major roles in signaling and membrane formation, which are required for cellular protrusions and invasive behaviors (44). Our lipidomics data suggest that melanomas can take up a complex mixture of multiple lipid species from adipocytes, including not solely long-chain fatty acids but also cholesterol, and it is likely that each of these lipids exerts specific effects on melanoma cell phenotypes.

One question that our study raises is the extent to which dietary factors and obesity play into the progression of melanoma. The fatty-acid content of subcutaneous adipocytes is influenced by dietary consumption, and this will in turn influence which lipids are most readily transferred into the melanoma cells. Some but not all studies have shown a connection between obesity and increased risk of melanoma (45–51), and this effect may be gender related, because a recent study demonstrated that obese males being treated with immunotherapy or targeted therapies had a better outcome in melanoma compared with obese females (52). In addition, high-fat diets are known risk factors for melanoma progression (53–55). Whether changing the dietary intake of either the total amount of fat or the ratio of saturated to unsaturated fats could prevent some early-stage melanomas from progressing to metastatic disease will be a question of great interest for future studies.

METHODS

Cell Lines

A375 and SKMel28 cells were obtained in August 2013 from the ATCC, which performs routine cell line authentication testing using morphology, karyotyping, and PCR-based methods including short-tandem repeat profiling to confirm the identity of human cell lines and to rule out interspecies contamination. The cells were also routinely tested for *Mycoplasma* using a luminescence-based assay (Mycoalert Mycoplasma Detection Kit, Lonza), most recently in March 2017. Cells were passaged no more than 25 times before a low-passage batch was thawed. ZMEL1 cells were established previously in the lab in 2012 and underwent routine *Mycoplasma* testing, most recently in March 2017.

Zebrafish Husbandry

All zebrafish experiments were carried out in accordance with institutional animal protocols. All zebrafish were housed in a temperature (28.5°C) and light-controlled (14 hours on, 10 hours off) room. Fish were initially housed at a density of 5 to 10 fish per liter and fed 3 times per day using brine shrimp and pelleted zebrafish food. After transplantation, the fish were housed in individual chambers for serial imaging. All anesthesia was done using Tricaine (Western Chemical Incorporated) with a stock of 4 g/L (protected for light) and diluted until the fish was immobilized. All procedures were approved by and adhered to Institutional Animal Care and Use Committee (IACUC) protocol #12-05-008 through Memorial Sloan Kettering Cancer Center.

Mouse Xenografts

All mouse experiments were carried out in accordance with institutional animal protocols. A375 cells (7×10^6) were suspended in 200 μL Matrigel (BD Bioscience) and injected subcutaneously into the left and right flanks of 6-week-old female athymic nude *Foxn1nu* mice (The Jackson Laboratory). Tumor growth was monitored using caliper measurements, and tumor volume was calculated using the formula 3.14159 × length × width 2/6,000. Mice were sacrificed by CO_2 asphyxiation when tumor size exceeded 2,000 mm^3. Statistical analysis between A375-mCherry and A375-FATP1-mCherry groups was determined using two-way ANOVA with multiple comparisons. All procedures were approved by and adhered to IACUC protocol #04-03-009 through Memorial Sloan Kettering Cancer Center.

ZMEL1-GFP Adult Transplants

Adult Casper fish between 4 and 9 months old were anesthesized with Tricaine and transplanted with 5×10^5 ZMEL1 cells suspended in 3 μL PBS in the subcutaneous tissue directly before the anal fin on the lateral side of the fish using a Hamilton 26s gauge, bevel tip syringe (Sigma, cat no. 20734). After transplant, fish were returned to water to recover and maintained on system for indicated times.

Generation of the FATP1 MinicoopR Transgenic

Experiments were performed as outlined in ref. 24. Briefly, *Trp53/BRAF/Nacre* embryos were injected with 25 ng/μL of either *MiniCoopR* alone or *MiniCoopR;mitf:FATP1* (along with 20 ng/μL of Tol2 transposase mRNA) and selected for melanocyte rescue at 48 hours. Melanocyte-rescued embryos were grown to adulthood ($n = 29$ for control and $n = 27$ for *mitf:FATP1*) and scored for the emergence of raised melanoma lesions as per ref. 24 at 16 weeks after fertilization.

Generation of the Plin2:tdTomato Transgenic

Zebrafish *Plin2* promoter fragment was amplified from zebrafish genomic DNA with 5′-cactgcattgaagagaaaatacaataac-3′ forward primer and 5′-GTTAGCAGAAAATctgcaaaagaaaatag-3′ reverse primer and introduced into a Gateway destination vector in the Tol2Kit that generated a *Plin2:tdTomato* cassette. This plasmid was injected into Casper embryos with Tol2 mRNA to introduce stable integration of the *Plin2:tdTomato* cassette.

In Vivo *Lipofermata* Treatment

Adult Casper fish between 4 and 9 months old were anesthesized with Tricaine and transplanted with 3×10^5 ZMEL1 cells suspended in 3 μL PBS in the subcutaneous tissue directly before the anal fin on the lateral side of the fish using a Hamilton 26s gauge, bevel tip syringe (Sigma, cat no. 20734). After transplant, fish were returned to water to recover and maintained on system. At 5 DPT, when successfully engrafted tumors were visible to the naked eye, 5 μmol/L of Lipofermata or 0.01% DMSO was injected directly into the tumor with a borosilicate needle once a day. Fish were imaged using a Zeiss AxioZoom at 5 days after treatment with GFP and brightfield channels on the left and right sides of each animal. Each image was imported from the Zeiss Zen software as a TIFF and analyzed in ImageJ. To measure tumor area, GFP^+ tumor was segmented using the default ImageJ segmentation algorithm and thresholding applied uniformly across all groups.

Downloaded from http://aacrjournals.org/cancerdiscovery/article-pdf/8/8/1006/1841481/1006.pdf by guest on 27 August 2022

To measure total lipid content in tumors treated with Lipofermata, fish were treated as stated above and then sacrificed 5 days after treatment. The tumor was dissected from the fish and then FACS isolated. Post-FACS, DMSO or Lipofermata-treated tumor cells were washed 1× with PBS, then stained with LipidTOX Red as described below.

3T3L1 Maintenance and Differentiation into Adipocytes

3T3L1 cells were obtained from ZenBio and culture and differentiation were performed according to the manufacturer's instructions. Briefly, cells were grown on various culture dishes until 2 days after 100% confluency in preadipocyte media (ZenBio, cat no. PM-1-L1). Two days after confluency, media were changed to differentiation medium (ZenBio, cat no. DM-2-L1) and incubated for 5 days. Then, cells were maintained in their adipocytic, differentiated state with maintenance media (ZenBio, cat no. AM-1-L1). This adipocyte maintenance media (ZenBio, cat no. AM-1-L1) was used for all coculture experiments.

FATP1 Expression Analysis

Expression of FATP1/SLC27A1 was examined using the Broad Institute Cancer Cell Line Encyclopedia database as well as the Oncomine Database. Within the Broad Institute portal, the RNA-seq mRNA expression levels for each tumor subtype were averaged across the 1,019 cancer cell lines, which includes 63 melanoma samples. For Oncomine, we used the default parameters to examine enrichment in the "Cancer vs. Cancer" data analysis tool, which showed enrichment of SLC27A1 only in melanoma and no other tumors.

Quantitative RT-PCR

Total RNA was isolated directly from cultured cells using the Quick-RNA Miniprep Kit (Zymo, R1054). Reverse transcription was performed with Superscript III First-Strand Synthesis System (Thermo-Fisher 18080). *FATP1* mRNA levels were measured with 5′-TGACAGTCGTCCTCCGCAAGAA-3′ and 5′-CTTCAGCAGG TAGCGGCAGATC-3′ primers using the iQ SYBR Green Supermix (Bio-Rad) on a Bio-Rad CFX384-Touch System (Bio-Rad). Relative expression levels were normalized to beta-actin.

Lipid Visualization and Quantification

Live Staining and Imaging of Zebrafish with BODIPY. To image lipids in melanoma *in vivo*, adult fish bearing ZMEL1-GFP tumors were stained with BODIPY as previously described (56, 57). Briefly, 21 DPT fish were stained with BODIPY 558/568 at a working concentration of 2 μg/mL in fish water for 1 hour in the dark. Fish were rinsed briefly in fresh fish water, and then placed on system with running water for 2 hours. After staining, fish were anesthetized with Tricaine and placed onto a petri dish. The fish were imaged from above using a Zeiss AxioZoom V16 Fluorescence Stereo Zoom Microscope with a 0.6 × or 1.6 × adjustable objective lens. Each fish was successively imaged using brightfield, GFP, and tdTomato filter sets on both sides. To image lipids in non–adipocyte-rich areas, 2 days after fertilization fish were transplanted with ZMEL1-GFP cells as previously described (20) and allowed to engraft and grow for 3 DPT. Embryos were then stained with BODIPY as previously described (56, 57). After staining, fish were anesthetized and imaged as described above, focusing on ZMEL1-GFP cells in the tail region of the animal. Differences in colocalization of the BODIPY and GFP signal between adipocyte-rich versus adipocyte poor areas were calculated using χ^2 statistics.

LipidTOX Staining and Quantification. To measure total lipid content in ZMEL1-GFP cells *in vivo*, fish were transplanted as described above and then allowed to grow to 5 or 21 DPT, when fish were dissociated using Trypsin and ZMEL1-GFP cells were FACS isolated. To measure total lipid content in melanoma cells after coculture, GFP$^+$ human and fish melanoma cells were cultured with 3T3L1 adipocytes for 7 days, then FACS isolated. After FACS, cells in all conditions were washed 1× with PBS, then stained with LipidTOX Red (Invitrogen) at a 1:125 dilution in DMEM-10 for 30 minutes at room temperature protected from light. Cells were washed 2× with PBS, then diluted to similar concentrations in PBS and mounted in a disposable hemocytometer for imaging. More than 10 fields per condition were imaged with a Zeiss AxioImager with a 20× fixed objective in the GFP and mCherry channels. Signal intensity of LipidTOX Red was measured in each field in GFP$^+$ cells and quantified in ImageJ.

Transmission Electron Microscopy. For human cell lines, FACS-isolated melanoma cells grown in coculture with 3T3L1 adipocytes for 7 days were 4% paraformaldehyde, 2.5% glutaraldehyde, 0.002% picric acid in 0.1 mol/L sodium cacodylate buffer, pH 7.3 for transmission electron microscopy (12,000–15,000×). For electron microscopy in fish, ZMEL1-GFP cells were transplanted into adult Casper fish and grown until 21 DPT, when they were sacrificed in an ice bath. Tumors were resected from fish and fixed in fix solution described above, then processed for imaging. Imaging was performed on the JEOL JSM 1400, operated at 100 kV. Images were captured on a Veleta 2K × 2K CCD camera (EM-SIS). Quantification of lipid droplet number and size were performed using ImageJ software with 10 cells/condition.

Proliferation Assays

To measure cell proliferation after Lipofermata treatment, SKMEL-28, A375, and ZMEL1 cells were plated at a density of 4,000 to 20,000 cells per well in a 96-well plate in 100 μL of DMEM-10. Cells were allowed to adhere for 24 hours, and then media changed to fresh media containing either DMSO, Lipofermata, or its inactive analogue CB16.6 at the indicated doses. The final concentration of all wells contained equivalent amounts of DMSO solvent (1%). After 48 hours of Lipofermata treatment, CellTiter-Glo reagent (Promega) was added to cells per the manufacturer's instructions and luminescence was read using a BioTek Synergy 96-well plate reader. All values were normalized to the DMSO control well, done in triplicate for all cell lines.

For phospho-Histone H3 staining, 3T3L1 cells were seeded and differentiated onto 4- or 8-well MilliCell slides (Millipore). Once 3T3L1 cells were fully differentiated into adipocytes, 10,000 to 20,000 A375-GFP or SKMel28-GFP cells were plated in either DMEM-10 or DMEM-0 media. Cells were fixed in fresh 4% paraformaldehyde and stained with a phospho-Histone H3 primary antibody (1:1,000; Millipore; cat no. 05-806) and AlexaFluor-594–conjugated anti-mouse secondary antibody (1:1,000; Thermo Fisher Scientific). Slides were imaged on a Zeiss AxioImager inverted widefield fluorescence microscope. More than 10 images were acquired for all conditions. The number of mitotic cells was quantified by calculating double-positive cells (GFP$^+$, AlexaFluor594$^+$) as a fraction of the total number of GFP$^+$ cells in each field.

To test the effects of lipid supplementation, 4,000 A375 cells/well were seeded onto 96-well plates in DMEM-10 and allowed to adhere overnight. The next day, media were aspirated from plates and replaced with serum-free or glucose-free DMEM with or without supplementation with 1:100 Lipid Mixture 1 (Sigma-Aldrich; cat no. L0288). At 24, 48, and 72 hours after treatment, cells were quantified using Cyquant Direct Cell Proliferation Assay (Thermo Fisher Scientific) according to the manufacturer's instructions.

Drug Treatments in Monocultured versus Cocultured Cells

A375-GFP cells were seeded on MilliCell slides in monoculture or in coculture with adipocytes and allowed to adhere overnight. The next day, media were replaced by media containing either 1% DMSO,

Downloaded from http://aacrjournals.org/cancerdiscovery/article-pdf/8/8/1006/1841481/1006.pdf by guest on 27 August 2022

1.25 to 5 μmol/L Lipofermata, or 12.5 to 50 μmol/L cerulenin. After 48 hours, cells were fixed and mounted for imaging. Cells were imaged with a Zeiss AxioImager with a 20× fixed objective in the GFP+ channel. More than 3 images were acquired for all conditions. Quantification of BODIPY in melanoma cells was performed using ImageJ software by calculating the total fluorescence area in the GFP+ channel in control- versus drug-treated samples.

Lipid Uptake Assays

SKMel28, A375, and ZMEL1 cells were seeded at a density of 10,000 to 20,000 cells per well in a 96-well plate in 100 μL DMEM-10. Cells were allowed to adhere and grow to 95% to 100% confluence for 2 days. To test the effect of Lipofermata, cells were starved for 1 hour in DMEM-0. After 1 hour, media were removed and replaced with fresh DMEM-10 media with either DMSO, Lipofermata, or CB16.6 at the indicated doses. After treatment for 1 hour, fatty-acid transport kinetics were evaluated according to the method described in Arias-Barrau and colleagues (58). Briefly, after 1 hour of Lipofermata or CB16.6 treatment, C1-BODIPY-C12 or BODIPY-C16 uptake was measured using a BioTek Synergy plate reader immediately after adding the C1-BODIPY-C12 or BODIPY C16 substrate to cells. The substrate was presented to the cells as a complex with fatty acid–free BSA to give BODIPY-FA to BSA ratios of 4:1 (5 μmol/L C1-BODIPY-C12 or 0.6–5 μmol/L BODIPY-C16 and 5 μmol/L BSA). Non–cell-associated fluorescence was quenched with Trypan blue. Uptake was measured at 485 nm excitation and 528 nm emission.

For the timed measurement of fatty-acid uptake in FATP-overexpressing and FATP CRISPR cells, cells were seeded into 96-well plates and grown as described above. Lipid uptake was measured with the QBT Fatty Acid Uptake Assay (Molecular Devices) using the BioTek Synergy plate reader. Fluorescence at 485 nm excitation and 528 nm emission was measured every 50 seconds for 1 to 2 hours. For the timed measurement of fatty-acid uptake in FATP-overexpressing and FATP1 CRISPR A375 cells treated with Lipofermata, cells were seeded into 96-well plates and grown as described above. To test the effect of Lipofermata and CB16.6, cells were starved for 1 hour in fresh DMEM-10 with either DMSO, Lipofermata, or CB16.6 at the indicated doses. After treatment, lipid uptake was measured with the QBT Fatty Acid Uptake Assay every 50 seconds for 1 to 2 hours.

Lipid Transfer Experiments

The 3T3L1 cells were seeded onto 4-well EZ MilliCell slides (EMD Millipore PEGZ0416) and differentiated according to the manufacturer's instructions (ZenBio). Lipids in adipocytes were labeled with 5 μmol/L BODIPY 558/568 C-12 or BODIPY C-16 in adipocyte maintenance media (ZenBio) for 4 hours. After 4 hours, extracellular BODIPY was removed from the cells by washing three times with 1× Hank's Balanced Salt Solution with 0.2% fatty acid–free BSA. After washing, GFP+ human and zebrafish melanoma cells were seeded on top of labeled adipocytes for 24 hours. Cells were then fixed and imaged on a Zeiss AxioImager, where BODIPY-laden GFP+ melanoma cells could be observed. To test whether lipid transfer required direct cell–cell contact and the effect of Lipofermata on lipid uptake, 3T3L1 cells were grown and differentiated on the top chamber of a Transwell system (Corning) and labeled with BODIPY as described above. In a separate well, GFP+ melanoma cells were plated onto a 12-mm circular coverslip in a separate well and allowed to adhere. After 4 hours of BODIPY labeling, 3T3L1 adipocytes were washed as described above, and the transwells containing BODIPY-labeled adipocytes were transferred to wells containing GFP+ melanoma cells on a coverslip. The melanoma cells on the bottom of the well on a coverslip were cocultured with the adipocytes on the top, separated by the Transwell, for 24 hours, in the presence of either 2.5 μmol/L Lipofermata or DMSO. Melanoma cell slides were then fixed and mounted onto slides. Slides were imaged on a Zeiss AxioImager inverted widefield fluorescence microscope. More than 10 images were acquired for all conditions. Quantification of BODIPY in melanoma cells was performed using ImageJ software by calculating the total fluorescence intensity in GFP+ cells in control- versus Lipofermata-treated samples.

RNA-seq of ZMEL1

The zebrafish ZMEL1 data are adapted from our previous publication (8). Total RNA was isolated using the Zymo RNA isolation kit after FACS. Because the amount of starting material was small, the RNA was amplified using the NuGen RNA kit, after which the samples were sequenced on an Illumina HiSeq2500. Samples were sequenced using the HiSeq2500 with approximately 20 million reads per sample, using 50 bp single-end reads. Reads from each RNA-seq run were mapped to the zebrafish reference genome version danRer7 from the UCSC Genome Browser using GSNAP and quantified on the gene level using HTSeq and Ensembl version 75. Differential expression analysis was performed using DESeq2. The zebrafish gene symbols were mapped to their human orthologs using the DIOPT tool (http://www.flyrnai.org/cgi-bin/DRSC_orthologs.pl). Genes with a corrected *P* value of less than 0.05 were considered statistically significant. To generate heat maps, log-transformed normalized counts were generated using the "rlog" transformation in the R package DESeq2 and plotted as mean-subtracted values for each gene using MATLAB (MathWorks). Pathway analysis was done using Ingenuity Pathway Analysis software (https://www.qiagenbioinformatics.com/products/ingenuity-pathway-analysis/) and the Gene Set Enrichment Analysis packages (http://software.broadinstitute.org/gsea/index.jsp) using the log2FC and FDR < 0.05.

RNA-seq of A375 Cells

A375-GFP cells were grown either in monoculture or in coculture with 3T3L1 adipocytes for 7 days in adipocyte maintenance medium (ZenBio AM-1-L1). Melanoma cells were then FACS isolated and processed for RNA sequencing. Total RNA was isolated using the Zymo RNA kit and used for cDNA synthesis and barcoding with Illumina adapters, followed by sequencing on the Illumina HiSeq2500. RNA-seq reads were mapped to a concatenated human (hg19) and mouse (mm10) genome. This approach was used to filter out any contaminating mouse reads from the coculture setting. The combined mapping was performed with STAR (v2.5.0a) using default parameters and the parameter "–outFilterMismatchNmax 0." Gene counts were assessed using the "–quantMode GeneCounts" parameter in STAR with a custom gff file combining the mm10 and hg19 genomes. The subsequent count matrix was subset for human genes and used as an input for the R package DESeq2 for normalization and differential gene expression. Default parameters were used in DESeq2 and differentially expressed genes were called using a base mean of 15, log2 fold change of ± 1, and an FDR of 5%. Volcano plots were generated with the R package ggplot2, and the heat map in Fig. 4D was generated using the package pheatmap (https://CRAN.R-project.org/package=pheatmap). All data can be found in the GEO database with accession number GSE114941.

Lipidomics

For human melanoma lipidomics, A375-GFP cells were grown either in monoculture or in coculture with 3T3L1 adipocytes for 7 days in adipocyte maintenance medium (ZenBio, cat no. AM-1-L1). Melanoma cells were then FACS isolated and processed for lipidomics. For lipidomics on fish melanoma cells *in vivo*, ZMEL1-GFP cells were transplanted into adult Casper zebrafish and grown for 21 days, when tumor-bearing fish were sacrificed and ZMEL1-GFP cells were FACS isolated and processed for lipidomics.

Global lipidomic profiling was performed by Metabolon. Lipids were extracted from samples using dichloromethane and methanol in a modified Bligh-Dyer extraction in the presence of internal

Downloaded from http://aacrjournals.org/cancerdiscovery/article-pdf/8/8/1006/1841481/1006.pdf by guest on 27 August 2022

standards with the lower, organic, phase being used for analysis. The extracts were concentrated under nitrogen and reconstituted in 0.25 mL of dichloromethane:methanol (50:50) containing 10 mmol/L ammonium acetate. The extracts were placed in vials for infusion-MS analyses, performed on a SelexION-equipped Sciex 5500 QTRAP using both positive and negative mode electrospray. Each sample was subjected to two analyses, with IMS-MS conditions optimized for lipid classes monitored in each analysis. The 5500 QTRAP was operated in MRM mode to monitor the transitions for over 1,100 lipids from up to 14 lipid classes. Individual lipid species were quantified based on the ratio of signal intensity for target compounds to the signal intensity for an assigned internal standard of known concentration. Lipid class concentrations were calculated from the sum of all molecular species within a class, and fatty-acid compositions were determined by calculating the proportion of individual fatty acids within each class. Fold change compared with the control situation was calculated by dividing the average of the (experimental/control) value, and statistical differences analyzed using a two-tailed unpaired *t* test.

Gelatin Degradation Assays

Coverslips were coated with Alexa 546-gelatin (1 mg/mL), crosslinked with 0.5% glutaraldehyde (Sigma), and washed three times with 1× sterile PBS. A layer of collagen I (0.5 mg/mL) is polymerized on top of the gelatin matrix, 4 hours at 37°C. A375-GFP cells were starved 4 hours before seeding on matrix with DMEM 4.5 g glucose L-glutamine, 0.8% BSA, and 0.5% FBS. Conditioned media from adipocytes cultivated 24 hours in ZenBio serum-free maintenance media (Zenbio AM-1-L1-SF) supplemented with 0.8% BSA and 0.5% FBS were collected and centrifuged for 5 minutes 1,000 × *g* to remove cell debris. Thirty thousand melanoma cells were seeded on coated coverslips and incubated with adipocyte starvation media or conditioned media or 30,000 adipocytes overnight, before fixation and staining. To test Lipofermata effect on matrix degradation, melanoma cells were seeded on the matrix as described above for 4 hours before adding DMSO or 1.5 μmol/L Lipofermata, and incubated overnight before fixation and staining. Coverslips were stained for DAPI to localize adipocytes. Microscopy was performed on LEICA DM5500 B with a LEICA DFC345 FX camera and a 100× oil objective. Matrix degradation was quantified with ImageJ software as previously shown (59).

For the ZMEL1 gelatin degradation assay, cells were grown in monoculture or in coculture with 3T3L1 adipocytes for 7 days in adipocyte maintenance media (Zenbio AM-1-L1) and then FACS isolated for GFP and plated onto gelatin-Cy3-coated coverslips crosslinked with 0.5% glutaraldehyde supplied in the QCM Gelatin Degradation Assay Kit (Millipore; cat. no ECM671) and incubated for 24 hours in DMEM-10 before fixation and staining.

Transwell Invasion Assay

A375-GFP cells in monoculture or cocultured with adipocytes were FACS isolated and then seeded onto Biocoat Matrigel Invasion chambers (Corning) at a density of 15,000 cells/well in serum-free DMEM-0. DMEM-10 was used in the wells of the companion plate as a chemoattractant. After 24 hours, cells were fixed, and cells remaining on the top section of the chamber were scraped away. Migrated cells were stained with DAPI and imaged. The number of cells migrated was counted with ImageJ.

Collagen Plug Assay

Collagen plug generation and protocol were adapted from Lopez and colleagues (60). Briefly, 2 mg/mL type I rat tail collagen (BD) was cross-linked with Alexa-546 to create a collagen gel. Gel was spread onto Transwell inserts (8-μm pore; Geiner Bio One) and polymerized at 37°C for 1 hour. Collagen gel matrices were then hydrated with DMEM (Life Technologies) supplemented with 50% FBS (Biomedia) for 4 hours. A375-GFP cells were starved in DMEM-0 for 4 hours, trypsinized, counted, and plated in the upper chamber of the Transwell insert. After 3 days, Transwell inserts were removed from the plate, and the quantity of invading cells into the gel matrix was determined by z-stack acquisition of GFP^+ cells with nuclei stained with DAPI.

Extracellular Flux Analysis of Melanoma Cells

Fatty-acid oxidation of melanoma cells previously cocultured with adipocytes for 7 days was determined through real-time measurement of the OCR using the XF96 Extracellular Flux Analyzer (Agilent Technologies), according to the manufacturer's instructions for the XF Fatty Acid Oxidation Assay. Briefly, FACS-isolated melanoma cells were seeded into XFp 96-well microplate wells at a density of 15,000 cells/well and incubated overnight for cells to adhere. One hour prior to loading the cell plate into the analyzer, cells were washed twice with 1× KHB buffer: (111 mmol/L NaCl, 4.7 mmol/L KCl, 1.25 mmol/L $CaCl_2$, 2 mmol/L $MgSO_4$, 1.2 mmol/L NaH_2PO_4) supplemented with 2.5 mmol/L glucose, 0.5 mmol/L carnitine, and 5 mmol/L HEPES on the day of the assay, adjusted to pH 7.4 at 37°C and maintained in KHB buffer in a CO_2-free 37°C incubator. Fifteen minutes prior to plate loading, etomoxir or vehicle was added to cells to a final concentration of 40 μmol/L, according to Agilent manufacturer's instructions, though other publications have used lower concentrations (61). OCR and ECAR were quantified following consecutive treatment of melanoma cells with four treatments: (i) assay medium alone, (ii) 2 μmol/L oligomycin, (iii) 2 μmol/L FCCP, and (iv) 0.5 μmol/L rotenone/antimycin A. For each assay, individual basal measurements were taken, followed by consecutive injection of treatments. Measurements were recorded after each injection, with each measurement consisting of 10-second mixing and 3-minute measurement period.

IHC and Oil Red O Staining on Patient-Derived Tumor Samples

IHC and Oil Red O for Cryopreserved Patient Biopsies and PDXs. Fresh tumors or PDX tumor samples were obtained and immediately frozen in OCT in cryomolds. Serial 4-μm sections from each sample were cut using a cryostat (Leica). Immunohistochemistry was performed by HistoWiz Inc. on a Bond Rx autostainer (Leica Biosystems). Each sample was stained for Oil Red O and FATP1 (1:100; Biorbyt orb336775). All primaries were detected using Polymer HRP followed by DAB. All the sections were then counterstained with hematoxycilin, dehydrated, and film-coverslipped using a TissueTek-Prisma and Coverslipper (Sakura). Whole-slide scanning (40×) was performed on an Aperio AT2 (Leica Biosystems). For FATP1/Oil Red O quantification, 3 to 5 similar regions of serial sections on Oil Red O and FATP1 patient slides were collected using ImageScope (Leica Biosystems). RGB images were converted to an HSB Stack Splitter plugin in ImageJ. Areas of positive Oil Red O or FATP1 staining were quantified for each sample (revealed in the Saturation channel) and quantified as a percentage of total tumor area (revealed in the Brightness channel). For adipocyte size quantification, the maximal length of 10 to 20 adipocytes either directly adjacent to tumor or not adjacent to tumor was measured using ImageJ.

IHC on Tumor Microarrays. Tumor microarrays (TMA) were obtained from the Memorial Sloan Kettering Cancer Center TMA Database and US Biomax (ME1007). Immunohistochemistry was performed by HistoWiz Inc. on a Bond Rx autostainer (Leica Biosystems). Each sample was stained for FATP1 (1:100; Biorbyt orb336775). Primaries were detected using Polymer-HRP followed by alkaline phosphatase. All the sections were then counterstained, dehydrated, film coverslipped, and scanned as described above.

Downloaded from http://aacrjournals.org/cancerdiscovery/article-pdf/8/8/1006/1841481/1006.pdf by guest on 27 August 2022

TMA and PDX Scoring. FATP1 staining was quantified by evaluating staining intensity (0–3 scale) and the percentage of positive cells (1:1%–24%, 2:25%–49%, 3:50%–74%, 4:75%–100%). The two values were multiplied together to obtain an integrated score ranging from 0 to 12. Each sample received a final score based on the integrated score. Final scores reflect integrated scores as follows:

0 = integrated score 0
1 = integrated score 1–3
2 = integrated score 4–7
4 = integrated score 8–12

IHC on Transplanted Casper Fish. Adult Casper fish were transplanted with ZMEL1-GFP cells as described above. At 18 DPT, fish were sacrificed in an ice-water bath and fixed for 48 hours in 4% paraformaldehyde at 4°C. After fixation, fish were washed and incubated in 70% ethanol until paraffin embedding (HistoWiz). Sagittal sections (5 μm) were collected for the left and right sides of each fish as well as 5-μm sections in the center of the fish. Each section was stained with anti-GFP antibody to visualize metastases. Each slide was scored for total metastases and number of metastases occurring next to adipocytes.

Caspase 3/7 Assay

Cells were plated onto 96-well plates at a seeding density of 20,000 cells/well and grown for 2 days until confluent. 1.5 μmol/L, 5 μmol/L and 10 μmol/L Lipofermata or DMSO was added to cells for 24 hours. Caspase 3/7 reagent (Promega) was then added to cells and luminescence was read out on a Synergy H1 plate reader according to the manufacturer's instructions.

Generation of FATP-Overexpressing Cell Lines

A375-FATP1-mCherry and A375-mCherry cells were generated via viral transduction. To generate lentiviruses, viral expression plasmids containing CMV-FATP1-mCherry or CMV-mCherry alone were transfected into HEK293T cells at 90% confluency in 10-cm dishes along with pMDG2 and psPAX2 packaging plasmids using Lipofectamine 2000. Six hours after transfection, the media were replaced with 6 mL DMEM-30. Virus-containing supernatants were collected 24 hours later and passed through a 0.45-μm filter to eliminate cells and debris. A375 cells at 80% confluency in 6-well plates in the presence of 1 μg/mL polybrene (Millipore) were infected with 100 μL virus in a total of 1 mL media volume. Twenty-four hours after transduction, virus-containing media were removed, and cells were maintained for two passages. mCherry-positive cells were selected using FACS with the same gates to ensure similar transgene expression.

Generation of FATP1 CRISPR Knockout Cells

FATP1 was knocked out of A375 cells following the technique described by Ran and colleagues (62). Briefly, a single-guide RNA (sgRNA) expression construct was generated for *FATP1*. Oligonucleotides for top and bottom strands of the sgRNA were phosphorylated with T4 PNK (New England Biolabs), annealed, and then cloned into the dual Cas9/sgRNA expression vector pSpCas9n(BB)-2A-GFP (Addgene 48140, kindly deposited by F. Zhang; ref. 62). Validated expression constructs were transfected into A375 cells with Lipofectamine 2000 (Thermo Fisher Scientific). GFP^+ cells were FACS isolated and plated as single cells into 96-well plates to generate single-cell clones. To identify clones that were successfully edited, genomic DNA was isolated from each clone and the genomic region targeted by each sgRNA was amplified via PCR, cloned into pCRII-TOPO via TOPO-TA cloning (Thermo Fisher Scientific), then Sanger sequenced. Cell lines were identified for *FATP1* with insertions or deletions near the predicted PAM site (underlined) that led to frameshift mutations.

FATP1 sgRNA1 target	5′-CCGTCACCTGCTGTGCACGACAA-3′
FATP1 sgRNA2 target	5′-CCGGCGGCGCTCGGCGTGTACGT-3′

^{13}C-Labeling and LC/MS Analysis of Lipid Synthesis in A375 cells

A375-GFP cells were cocultured with adipocytes for 6 days, then FACS isolated. These cells were then replated as monocultures in adipocyte maintenance media (ZenBio) that was supplemented with 10 mmol/L ^{13}C-acetate (Cambridge Isotopes, cat no. CLM-440-1). After 24 hours of ^{13}C treatment, the cells were then processed for LC/MS: cells were washed in-well with 1 mL of cold 0.9% NaCl. After consecutive addition of 600 μL of LC/MS grade methanol and 300 μL of LC/MS grade water, cells were scraped off and 750 μL of the suspension was mixed with 400 μL of LC/MS grade chloroform for nonpolar metabolites extraction. After 10 minutes of extraction by vortexing at 4°C and centrifugation for 10 minutes at 10,000 × *g* at 4°C, 350 μL of the lower lipid-containing layer was carefully collected and dried under nitrogen. Dried lipid extracts were stored at −80°C until LC/MS analysis. The dried samples were resolubilized in 50 μL of a 4:3:1 mixture (isopropanol:acetonitrile:water) and analyzed by UPLC/MS-MS with a polarity switching method modified from Vorkas and colleagues (63–65). The LC column was a Waters CSH-C18 (2.1 × 100 mm, 1.7 μm) coupled to a Dionex Ultimate 3000 system, and the column oven temperature was set to 55°C for the gradient elution. The flow rate of 0.3 mL/minute was used with the following buffers: A, 60:40 acetonitrile:water, 10 mmol/L ammonium formate, and 0.1% formic acid, and B, 90:10 isopropanol:acetonitrile, 10 mmol/L ammonium formate, and 0.1% formic acid. The gradient profile was as follows; 40%–43% B (0–1.25 minutes), 43%–50% B (1.25–2 minutes), 50%–54% B (2–11 minutes), 54%–70% B (11–12 minutes), 70%–99% B (12–18 minutes), 70%–99% B (18–32 minutes), 99–40% B (23–24 minutes), hold 40% B (1 minute). Injection volume was set to 1 μL for all analyses (25 minutes total run time per injection).

MS analyses were carried out by coupling the LC system to a Thermo Q Exactive HF mass spectrometer operating in heated electrospray ionization mode (HESI). Method duration was 20 minutes with a polarity switching data-dependent Top 10 method for both positive and negative modes. Spray voltage for both positive and negative modes was 3.5 kV and capillary temperature was set to 320°C, with a sheath gas rate of 35, aux gas of 10, and max spray current of 100 μA. The full MS scan for both polarities utilized 120,000 resolution with an AGC target of 3×10^6 and a maximum IT of 100 ms, and the scan range was from 350 to 2,000 m/z. Tandem MS spectra for both positive and negative modes used a resolution of 15,000, AGC target of 1×10^5, maximum IT of 50 ms, isolation window of 0.4 m/z, isolation offset of 0.1 m/z, fixed first mass of 50 m/z, and 3-way multiplexed normalized collision energies (nCE) of 10, 35, and 80. The minimum AGC target was 5×10^4 with an intensity threshold of 1×10^6. All data were acquired in profile mode.

The resulting lipids were identified by searching the LipidBlast tandem mass spectral library of lipids (66). The top scoring structure match for each data-dependent spectrum was returned using an in-house script for MSPepSearch_x64. Putative lipids were sorted from high to low by their reverse dot scores, and duplicate structures were discarded, retaining only the top-scoring MS2 spectrum and the neutral chemical formula, detected m/z, and detected polarity (+ or −) of the putative lipid was recorded. The relative intensities of these lipids (M+0 ion) were quantified at 10 ppm tolerance using an in-house script. Top lipid hits (e.g., PC 34:1) were manually examined by MS1, and significant ^{13}C-acetate labeling was observed. The intensity of each isotopolog in the PC 34:1 envelope was extracted using the theoretical mass of the M+0 through M+34 ions (M+1

Downloaded from http://aacrjournals.org/cancerdiscovery/article-pdf/8/8/1006/1841481/1006.pdf by guest on 27 August 2022

plus increments of 1.00335 representing addition of a ^{13}C atom). For a given isotopolog window (mono or co samples), the isotopolog intensities were converted to relative intensity with respect to the M+0, i.e., monoisotopic peak. Unpaired multiple *t* tests (corrected for multiple comparisons using the Holm–Sidak method) for each isotopomer were carried out to determine if the total amount of ^{13}C-acetate incorporation was significantly different between mono and co samples.

Statistical Analysis and Data Reproducibility

All statistical analysis was performed using GraphPad Prism Pro5 unless otherwise noted. Data are presented as mean ± standard error (SEM) unless stated otherwise in each figure legend. $P < 0.05$ was considered statistically significant. All *in vitro* experimenters were repeated in at least triplicate to ensure enough variation and numbers to measure significance by unpaired *t* tests as indicated in the legends. For *in vivo* experiments, *n* denotes either number of animals or independent experiments, as indicated in each figure legend. Experiments were repeated in at least triplicate to ensure enough variation and numbers to measure significance by unpaired *t* tests as indicated in the legends.

To ensure randomization of measurements used in image analysis, ≥10 fields/condition were acquired for each independent experiment. For zebrafish experiments, all fish were analyzed, with no randomization or blinding. Sex of fish was randomized.

Data Availability

We will make materials, data, code, and associated protocols available to readers promptly and without undue qualifications. All RNA-seq data will be uploaded to the Gene Expression Omnibus database (accession #GSE114941).

Disclosure of Potential Conflicts of Interest

C.E. Ariyan is a consultant/advisory board member for Bristol-Myers Squibb. No potential conflicts of interest were disclosed by the other authors.

Authors' Contributions

Conception and design: M. Zhang, R.M. White
Development of methodology: M. Zhang, J.S. Di Martino, V. Yong-Gonzales, T. Hollmann, R.M. White
Acquisition of data (provided animals, acquired and managed patients, provided facilities, etc.): M. Zhang, N.R. Campbell, S.C. Baksh, T. Simon-Vermot, I.S. Kim, P. Haldeman, C. Mondal, V. Yong-Gonzales, T. Merghoub, D.R. Jones, X.G. Zhu, C.E. Ariyan, K. Birsoy, T. Hollmann, J.J. Bravo-Cordero, R.M. White
Analysis and interpretation of data (e.g., statistical analysis, biostatistics, computational analysis): M. Zhang, J.S. Di Martino, R.L. Bowman, N.R. Campbell, S.C. Baksh, D.R. Jones, A. Arora, J.D. Wolchok, K.S. Panageas, J.J. Bravo-Cordero, R.M. White
Writing, review, and/or revision of the manuscript: M. Zhang, S.C. Baksh, C.E. Ariyan, J.D. Wolchok, J.J. Bravo-Cordero, R.M. White
Administrative, technical, or material support (i.e., reporting or organizing data, constructing databases): M. Zhang, J.S. Di Martino, M. Abu-Akeel, R.M. White
Study supervision: M. Zhang, R.M. White

Acknowledgments

The authors would like to thank Wenjing Wu for assistance with illustrations, Andreas Stahl for important discussions/reagents, and Lee Cohen-Gould and Juan Jimenez for help with transmission electron microscopy. We would also like to thank Histowiz, Metabolon, and Genewiz for help with immunohistochemistry, lipidomics, and RNA-seq, respectively. Further, we thank Rebecca Rose in the NYU Metabolomics Core for performing LC/MS. This work was supported by the NIH Director's New Innovator Award (DP2CA186572), Mentored Clinical Scientist Research Career Development Award (K08AR055368), the Melanoma Research Alliance, The Pershing Square Sohn Foundation, The Alan and Sandra Gerry Metastasis Research Initiative at the Memorial Sloan Kettering Cancer Center, The Harry J. Lloyd Foundation, Consano, and the Starr Cancer Consortium (all to R.M. White). M. Zhang is supported by the Memorial Sloan Kettering Translational Research Oncology Training Program fellowship and National Cancer Institute F32 Postdoctoral Training Grant (CA210536-01A1). J.J. Bravo-Cordero is funded by an NCI Career Transition Award (K22CA196750) and the TCI Young Scientist Cancer Research Award JJR Fund (P30-CA196521). N.R. Campbell is supported by the Kirschstein-NRSA predoctoral fellowship (F30) under award number F30CA220954, by a research grant from the Melanoma Research Foundation, and by a Medical Scientist Training Program grant under award number T32GM007739.

Received December 5, 2017; revised April 6, 2018; accepted June 6, 2018; published first June 14, 2018.

REFERENCES

1. Quail DF, Bowman RL, Akkari L, Quick ML, Schuhmacher AJ, Huse JT, et al. The tumor microenvironment underlies acquired resistance to CSF-1R inhibition in gliomas. Science 2016;352:aad3018.
2. Tammela T, Sanchez-Rivera FJ, Cetinbas NM, Wu K, Joshi NS, Helenius K, et al. A Wnt-producing niche drives proliferative potential and progression in lung adenocarcinoma. Nature 2017;545:355–9.
3. Hodi FS, O'Day SJ, McDermott DF, Weber RW, Sosman JA, Haanen JB, et al. Improved survival with ipilimumab in patients with metastatic melanoma. N Engl J Med 2010;363:711–23.
4. Larkin J, Chiarion-Sileni V, Gonzalez R, Grob JJ, Cowey CL, Lao CD, et al. Combined nivolumab and ipilimumab or monotherapy in untreated melanoma. N Engl J Med 2015;373:23–34.
5. Tirosh I, Izar B, Prakadan SM, Wadsworth MH, Treacy D, Trombetta JJ, et al. Dissecting the multicellular ecosystem of metastatic melanoma by single-cell RNA-seq. Science 2016;352:189–96.
6. Colegio OR, Chu N-Q, Szabo AL, Chu T, Rhebergen AM, Jairam V, et al. Functional polarization of tumour-associated macrophages by tumour-derived lactic acid. Nature 2014;513:559–63.
7. Kaufman CK, Mosimann C, Fan ZP, Yang S, Thomas AJ, Ablain J, et al. A zebrafish melanoma model reveals emergence of neural crest identity during melanoma initiation. Science 2016;351:aad2197.
8. Kim IS, Heilmann S, Kansler ER, Zhang Y, Zimmer M, Ratnakumar K, et al. Microenvironment-derived factors driving metastatic plasticity in melanoma. Nat Commun 2017;8:14343.
9. Wang J, Chen G-L, Cao S, Zhao M-C, Liu Y-Q, Chen X-X, et al. Adipogenic niches for melanoma cell colonization and growth in bone marrow. Lab Invest 2017;97:737–45.
10. Wagner M, Bjerkvig R, Wiig H, Melero-Martin JM, Lin R-Z, Klagsbrun M, et al. Inflamed tumor-associated adipose tissue is a depot for macrophages that stimulate tumor growth and angiogenesis. Angiogenesis 2012;15:481–95.
11. Hollander DM, Devereux DF, Taylor CG, Taylor DD. Demonstration of lipolytic activity from cultured human melanoma cells. J Surg Res 1986;40:445–9.
12. Ellerhorst JA, Diwan AH, Dang SM, Uffort DG, Johnson MK, Cooke CP, et al. Promotion of melanoma growth by the metabolic hormone leptin. Oncol Rep 2010;23:901–7.
13. Lazar I, Clement E, Dauvillier S, Milhas D, Ducoux-Petit M, LeGonidec S, et al. Adipocyte exosomes promote melanoma aggressiveness through fatty acid oxidation: a novel mechanism linking obesity and cancer. Cancer Res 2016;76:4051–7.
14. Nieman KM, Kenny HA, Penicka CV, Ladanyi A, Buell-Gutbrod R, Zillhardt MR, et al. Adipocytes promote ovarian cancer metastasis

Downloaded from http://aacrjournals.org/cancerdiscovery/article-pdf/8/8/1006/1841481/1006.pdf by guest on 27 August 2022

and provide energy for rapid tumor growth. Nat Med 2011;17:1498–503.
15. Wang YY, Attané C, Milhas D, Dirat B, Dauvillier S, Guerard A, et al. Mammary adipocytes stimulate breast cancer invasion through metabolic remodeling of tumor cells. JCI Insight 2017;2:e87489.
16. Liberzon A, Subramanian A, Pinchback R, Thorvaldsdóttir H, Tamayo P, Mesirov JP. Molecular signatures database (MSigDB) 3.0. Bioinformatics 2011;27:1739–40.
17. Gazi E, Gardner P, Lockyer NP, Hart CA, Brown MD, Clarke NW. Direct evidence of lipid translocation between adipocytes and prostate cancer cells with imaging FTIR microspectroscopy. J Lipid Res 2007;48:1846–56.
18. Patton EE, Widlund HR, Kutok JL, Kopani KR, Amatruda JF, Murphey RD, et al. BRAF mutations are sufficient to promote nevi formation and cooperate with p53 in the genesis of melanoma. Curr Biol 2005;15:249–54.
19. White RM, Cech J, Ratanasirintrawoot S, Lin CY, Rahl PB, Burke CJ, et al. DHODH modulates transcriptional elongation in the neural crest and melanoma. Nature 2011;471:518–22.
20. Heilmann S, Ratnakumar K, Langdon E, Kansler E, Kim I, Campbell NR, et al. A quantitative system for studying metastasis using transparent zebrafish. Cancer Res 2015;75:4272–82.
21. Kazantzis M, Stahl A. Fatty acid transport proteins, implications in physiology and disease. Biochim Biophys Acta 2012;1821:852–7.
22. Anderson CM, Stahl A. SLC27 fatty acid transport proteins. Mol Aspects Med 2013;34:516–28.
23. Jönsson G, Busch C, Knappskog S, Geisler J, Miletic H, Ringnér M, et al. Gene expression profiling-based identification of molecular subtypes in stage IV melanomas with different clinical outcome. Clin Cancer Res 2010;16:3356–67.
24. Ceol CJ, Houvras Y, Jane-Valbuena J, Bilodeau S, Orlando DA, Battisti V, et al. The histone methyltransferase SETDB1 is recurrently amplified in melanoma and accelerates its onset. Nature 2011;471:513–7.
25. Sandoval A, Chokshi A, Jesch ED, Black PN, Dirusso CC. Identification and characterization of small compound inhibitors of human FATP2. Biochem Pharmacol 2010;79:990–9.
26. Ahowesso C, Black PN, Saini N, Montefusco D, Chekal J, Malosh C, et al. Chemical inhibition of fatty acid absorption and cellular uptake limits lipotoxic cell death. Biochem Pharmacol 2015;98:167–81.
27. Langley RR, Fidler IJ. The seed and soil hypothesis revisited–the role of tumor-stroma interactions in metastasis to different organs. Int J Cancer 2011;128:2527–35.
28. Massagué J, Obenauf AC. Metastatic colonization by circulating tumour cells. Nature 2016;529:298–306.
29. Quail DF, Joyce JA. Microenvironmental regulation of tumor progression and metastasis. Nat Med 2013;19:1423–37.
30. Balaban S, Shearer RF, Lee LS, van Geldermalsen M, Schreuder M, Shtein HC, et al. Adipocyte lipolysis links obesity to breast cancer growth: adipocyte-derived fatty acids drive breast cancer cell proliferation and migration. Cancer Metab 2017;5:1.
31. Iyengar P, Espina V, Williams TW, Lin Y, Berry D, Jelicks LA, et al. Adipocyte-derived collagen VI affects early mammary tumor progression in vivo, demonstrating a critical interaction in the tumor/stroma microenvironment. J Clin Invest 2005;115:1163–76.
32. Incio J, Liu H, Suboj P, Chin SM, Chen IX, Pinter M, et al. Obesity-induced inflammation and desmoplasia promote pancreatic cancer progression and resistance to chemotherapy. Cancer Discov 2016;6:852–69.
33. Laurent V, Guérard A, Mazerolles C, Le Gonidec S, Toulet A, Nieto L, et al. Periprostatic adipocytes act as a driving force for prostate cancer progression in obesity. Nat Commun 2016;7:10230.
34. Miranda F, Mannion D, Liu S, Zheng Y, Mangala LS, Redondo C, et al. Salt-Inducible kinase 2 couples ovarian cancer cell metabolism with survival at the adipocyte-rich metastatic niche. Cancer Cell 2016;30:273–89.
35. Dubois V, Delort L, Billard H, Vasson M-P, Caldefie-Chezet F. Breast cancer and obesity: in vitro interferences between adipokines and proangiogenic features and/or antitumor therapies? PLoS ONE 2013;8:e58541.
36. Chi M, Chen J, Ye Y, Tseng H-Y, Lai F, Tay KH, et al. Adipocytes contribute to resistance of human melanoma cells to chemotherapy and targeted therapy. Curr Med Chem 2014;21:1255–67.
37. Kwan HY, Fu X, Liu B, Chao X, Chan CL, Cao H, et al. Subcutaneous adipocytes promote melanoma cell growth by activating the Akt signaling pathway: role of palmitic acid. J Biol Chem 2014;289:30525–37.
38. Igal RA. Stearoyl CoA desaturase-1: new insights into a central regulator of cancer metabolism. Biochim Biophys Acta 2016;1861:1865–80.
39. Pascual G, Avgustinova A, Mejetta S, Martín M, Castellanos A, Attolini CS-O, et al. Targeting metastasis-initiating cells through the fatty acid receptor CD36. Nature 2017;541:41–5.
40. Baenke F, Peck B, Miess H, Schulze A. Hooked on fat: the role of lipid synthesis in cancer metabolism and tumour development. Dis Model Mech 2013;6:1353–63.
41. Qiu B, Ackerman D, Sanchez DJ, Li B, Ochocki JD, Grazioli A, et al. HIF2α-dependent lipid storage promotes endoplasmic reticulum homeostasis in clear-cell renal cell carcinoma. Cancer Discov 2015;5:652–67.
42. Hou NS, Gutschmidt A, Choi DY, Pather K, Shi X, Watts JL, et al. Activation of the endoplasmic reticulum unfolded protein response by lipid disequilibrium without disturbed proteostasis in vivo. Proc Natl Acad Sci U S A 2014;111:E2271–80.
43. Ackerman D, Simon MC. Hypoxia, lipids, and cancer: surviving the harsh tumor microenvironment. Trends Cell Biol 2014;24:472–8.
44. Huang P, Nedelcu D, Watanabe M, Jao C, Kim Y, Liu J, et al. Cellular cholesterol directly activates smoothened in hedgehog signaling. Cell 2016;166:1176–1187.e14.
45. Clement E, Lazar I, Muller C, Nieto L. Obesity and melanoma: could fat be fueling malignancy? Pigment Cell Melanoma Res 2017;30:294–306.
46. Karimi K, Lindgren TH, Koch CA, Brodell RT. Obesity as a risk factor for malignant melanoma and non-melanoma skin cancer. Rev Endocr Metab Disord 2016;17:389–403.
47. Samanic C, Gridley G, Chow W-H, Lubin J, Hoover RN, Fraumeni JF. Obesity and cancer risk among white and black United States veterans. Cancer Causes Control 2004;15:35–43.
48. Dobbins M, Decorby K, Choi BCK. The association between obesity and cancer risk: a meta-analysis of observational studies from 1985 to 2011. ISRN Prev Med 2013;2013:680536.
49. Tang JY, Henderson MT, Hernandez-Boussard T, Kubo J, Desai M, Sims ST, et al. Lower skin cancer risk in women with higher body mass index: the women's health initiative observational study. Cancer Epidemiol Biomarkers Prev 2013;22:2412–5.
50. Præstegaard C, Kjær SK, Christensen J, Tjønneland A, Halkjær J, Jensen A. Obesity and risks for malignant melanoma and non-melanoma skin cancer: results from a large Danish prospective cohort study. J Invest Dermatol 2015;135:901–4.
51. Fang S, Wang Y, Dang Y, Gagel A, Ross MI, Gershenwald JE, et al. Association between body mass index, C-reactive protein levels, and melanoma patient outcomes. J Invest Dermatol 2017;137:1792–5.
52. McQuade JL, Daniel CR, Hess KR, Mak C, Wang DY, Rai RR, et al. Association of body-mass index and outcomes in patients with metastatic melanoma treated with targeted therapy, immunotherapy, or chemotherapy: a retrospective, multicohort analysis. Lancet Oncol 2018;19:310–22.
53. Erickson KL. Dietary fat influences on murine melanoma growth and lymphocyte-mediated cytotoxicity. J Natl Cancer Inst 1984;72:115–20.
54. Jung JI, Cho HJ, Jung YJ, Kwon S-H, Her S, Choi SS, et al. High-fat diet-induced obesity increases lymphangiogenesis and lymph node metastasis in the B16F10 melanoma allograft model: roles of adipocytes and M2-macrophages. Int J Cancer 2015;136:258–70.
55. Pandey V, Vijayakumar MV, Ajay AK, Malvi P, Bhat MK. Diet-induced obesity increases melanoma progression: involvement of Cav-1 and FASN. Int J Cancer 2012;130:497–508.
56. Minchin JEN, Rawls JF. In vivo analysis of white adipose tissue in zebrafish. Methods Cell Biol 2011;105:63–86.
57. Minchin JEN, Rawls JF. In vivo imaging and quantification of regional adiposity in zebrafish. Methods Cell Biol 2017;138:3–27.

Downloaded from http://aacrjournals.org/cancerdiscovery/article-pdf/8/8/1006/1841481/1006.pdf by guest on 27 August 2022

58. Arias-Barrau E, Dirusso CC, Black PN. Methods to monitor Fatty Acid transport proceeding through vectorial acylation. Methods Mol Biol 2009;580:233–49.
59. Juin A, Di Martino J, Leitinger B, Henriet E, Gary A-S, Paysan L, et al. Discoidin domain receptor 1 controls linear invadosome formation via a Cdc42-Tuba pathway. J Cell Biol 2014;207:517–33.
60. Lopez JI, Camenisch TD, Stevens MV, Sands BJ, McDonald J, Schroeder JA. CD44 attenuates metastatic invasion during breast cancer progression. Cancer Res 2005;65:6755–63.
61. Yao C-H, Liu G-Y, Wang R, Moon SH, Gross RW, Patti GJ. Identifying off-target effects of etomoxir reveals that carnitine palmitoyltransferase I is essential for cancer cell proliferation independent of β-oxidation. PLoS Biol 2018;16:e2003782.
62. Ran FA, Cong L, Yan WX, Scott DA, Gootenberg JS, Kriz AJ, et al. In vivo genome editing using Staphylococcus aureus Cas9. Nature 2015;520:186–91.
63. Vorkas PA, Isaac G, Anwar MA, Davies AH, Want EJ, Nicholson JK, et al. Untargeted UPLC-MS profiling pipeline to expand tissue metabolome coverage: application to cardiovascular disease. Anal Chem 2015;87:4184–93.
64. Mirnezami R, Kinross JM, Vorkas PA, Goldin R, Holmes E, Nicholson J, et al. Implementation of molecular phenotyping approaches in the personalized surgical patient journey. Ann Surg 2012;255:881–9.
65. Vorkas PA, Shalhoub J, Isaac G, Want EJ, Nicholson JK, Holmes E, et al. Metabolic phenotyping of atherosclerotic plaques reveals latent associations between free cholesterol and ceramide metabolism in atherogenesis. J Proteome Res 2015;14:1389–99.
66. Kind T, Liu K-H, Lee DY, DeFelice B, Meissen JK, Fiehn O. LipidBlast in silico tandem mass spectrometry database for lipid identification. Nat Methods 2013;10:755–8.

Downloaded from http://aacrjournals.org/cancerdiscovery/article-pdf/8/8/1006/1841481/1006.pdf by guest on 27 August 2022